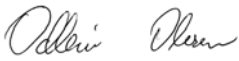


**NGU Report 2007.056**

**New insights into the West Siberian  
Basin from the satellite mission  
GRACE**

Report no.: 2007.056		ISSN 0800-3416	Grading: Confidential to 31.12.2009	
Title: New insights into the West Siberian Basin from the satellite mission GRACE				
Authors: Carla Braitenberg & Jörg Ebbing			Client: Statoil ASA	
County:			Commune:	
Map-sheet name (M=1:250.000)			Number of pages: 64	Price (NOK):
			Map enclosures:	
Fieldwork carried out:	Date of report: 31.08.2007	Project no.: 3133.00	Person responsible: 	
<p>Summary:</p> <p>The West Siberian Basin covers an area of <math>\sim 3.2 \times 10^6</math> km<sup>2</sup> and is among the most extended basins in the world. Recent investigations have revealed that the basin contains an extensive layer of flood basalts of late Permian-Triassic age, which have been set into relation to the basalts of the Siberian traps. In the northern parts of the basin, the basalts overly older sediments that reach locally over 15 km in thickness. Our work aims at reducing the observed gravity field to the basement level, estimating the contribution of the sediments and of the basalt layer to the gravity field. Published seismic sections with well-calibration are used for constraining the sediment isopachs and for estimating the density-depth functions. We also make use of published models on crustal thickness and basement depth and the gravity field derived from the integration of the satellite mission GRACE with terrestrial gravity measurements. The resulting 3D-density model is used for inferring density anomalies in the lower crust and upper mantle and allows calculating the total load acting on the crust and estimating the isostatic state of the region. A key question related to the formation of the basin is, whether a high density anomaly in the crust or upper mantle has contributed to the large scale subsidence of the basin, as has been postulated for other large scale basins. The lower crust shows considerable density variations, that allow making a segmentation of the basin into four blocks, the southern, mid, northern and north-western segments. We identify several rift structures and estimate the amount of basalt-filling. The eastern part of the basin towards the Siberian Platform shows an evident arch-shaped density increase in the lower crust, which is coincident with a rift extending for more than 1500 km length and bending into the Yenisey-Khatanga trough.</p>				
Keywords: Geophysics		Continental Shelf		Research
Gravimetry		Magnetometry		Isostasy
Report				

## CONTENTS

<b>1</b>	<b>Introduction</b> .....	<b>4</b>
1.1	Scope of the modeling .....	5
1.2	Temperature induced metamorphosis as a driving mechanism for subsidence .....	5
<b>2</b>	<b>Ages and geometry of the West Siberian Basin</b> .....	<b>7</b>
<b>3</b>	<b>Databases used in the study- present stage and upcoming data</b> .....	<b>11</b>
3.1	Gravity and topography data .....	11
3.2	Topographic correction of gravity and geoid fields .....	12
3.3	Moho depth .....	12
3.4	Basement depth and sediment layer .....	13
<b>4</b>	<b>Two-Way-Traveltime to depth conversion.</b> .....	<b>21</b>
4.1	Empirical TWT-depth and velocity-depth function .....	21
<b>5</b>	<b>Gravity and geoid fields</b> .....	<b>25</b>
5.1	Gravity anomaly and Bouguer anomaly .....	25
5.2	Geoid and terrain corrected geoid .....	26
5.3	Sediment gravity effect .....	26
5.4	Gravity effect of crustal thickness variations .....	27
5.5	Gravity effect of the basalt layer .....	29
<b>6</b>	<b>Gravity inversion</b> .....	<b>42</b>
6.1	Lower crustal density variations .....	42
6.2	Upper crustal density variations .....	43
6.3	Structural elements inferred from the inversion.....	44
<b>7</b>	<b>Isostatic state</b> .....	<b>48</b>
7.1	Isostatic crustal thickness .....	48
7.2	Isostatic gravity anomaly .....	48
<b>8</b>	<b>Conclusion and outlook</b> .....	<b>51</b>
	<b>Acknowledgements</b> .....	<b>57</b>
	<b>References</b> .....	<b>57</b>
	<b>Figures</b> .....	<b>62</b>

## 1 INTRODUCTION

The present report is the last in a series documenting results of a project studying the lithospheric setting and isostatic state of large scale- basins in general, and in detail for the Barents Sea and the West Siberian Basin.

Originally, the project started by studying the gravity field and the isostatic state of the Barents Sea Region. One of the main results was that the Eastern Barents Sea basins cannot be considered as typical rift basins, as they show distinctive features as large wavelengths, high lithospheric mantle density, thick sequence of sediments, a flat Moho and high elastic thickness, which are normally associated with cratonic or intracratonic basins (Ebbing et al. 2005, Ebbing et al. in press). We succeeded with a study of the general characteristics of large-scale basins and analysis the Michigan Basin in North America, the Solimões, Amazon, Parnaíba and Parana Basins in South America, the Tarim Basin in Central Asia and the Congo Basin in Africa in terms of gravity signal, geoid undulations, isostatic state, age and igneous activity.

All these basins showed similar deviation from the classic isostatic equilibrium model that predicts the crustal thickness from the topographic and sedimentary load. Instead of crustal thinning, high-density masses in the crust and mantle appeared to be a typical feature (Braitenberg and Ebbing 2006). An important point for the sediment evolution of the basins is the presence of the volcanism and the relative age of the volcanic strata with respect to the sedimentary package. In all the considered basins, except the Congo Basin, volcanic masses are present at some stage and at some depth in the basin.

Within the global study we also included the West Siberian Basin, which is one of the largest intracratonic basins of the world, and associated with extensive basalt layers. The present report gives now a more detailed image of the crustal structure of the lithosphere of the area, which is adjacent to the Barents Sea.

Future work will aim to link the results of the Barents Sea and West Siberia and to apply the knowledge gained by our studies to other largely, unknown studies in Africa and South America.

## **1.1 Scope of the modelling**

The object of study of the present research is the West Siberian Basin. The West Siberian Basin covers an area of 3.2-3.5  $10^6$  km<sup>2</sup> (Vyssotski et al. 2006) and is of great economic interest, due to the findings of huge oil and gas fields. Our study aims at the differentiation of the different basement units that are characterised by a diversification of the crustal structure. The extent of the basin is well defined (e.g. Vyssotski et al. 2006) when considering its limits towards the Urals (west) and towards the Siberian Platform (east). The termination of the basin northwards, and its transition to the Kara Sea, as well as northeastwards to the south of the Taimyr peninsula is also considered. Our study contributes a new element to the understanding of the basin, by using the newly acquired and developed GRACE gravity field derived from the dedicated gravity mission GRACE (Förste et al. 2006) with well developed and established methodologies (Braitenberg et al. 2003; Braitenberg and Ebbing 2006; Braitenberg and Ebbing 2007; Braitenberg et al. 2007a, 2007b; Ebbing et al. 2005; 2006; 2007; Shin et al. 2007; Wienecke et al. 2007). The field we use was obtained by integration of the satellite-derived data (down to half-wavelengths of 150 km) with terrestrial data, obtaining a field with 50 km half-wavelength resolution. The satellite-derived data have the advantage of global coverage independently of the ruggedness and remoteness of the terrain. Furthermore, the artificial signals possibly introduced by the combination of different measurement campaigns, a problem that can affect the long-wavelength part of the field, is overcome.

## **1.2 Temperature induced metamorphism as a driving mechanism for subsidence**

The West Siberian Basin has been set into relation to the North German Basin by Brink (2007) regarding a possible model for its development and evolution. The model gives considerable importance to geochemical and petrophysical processes in the lower crust to explain the subsidence of the basins. The authors find that the gravity field, reduced for the effect of sediments, has no correlation with the magnetic field anomalies. The latter have their origin above the 578 °C isothermal surface that corresponds to the Curie temperature of magnetite. For the North German Basin, the reduced gravity anomalies is supposed to correlate with the Curie temperature depth, assuming that shallowing of the Curie depth corresponds to a high gravity signal. Brink (2007) explains this fact to a metamorphic process, by which greenschist facies transform to amphibolite. The transformation is accompanied by

a 10% density increase from  $2700 \text{ kg/m}^3$  to  $3000 \text{ kg/m}^3$ , and a subsequent volume reduction. At a depth of 30 km, transformation is greatly temperature dependent and occurs accidentally at a value near to the Curie temperature of magnetite ( $578 \text{ }^\circ\text{C}$ ). For the North German Basin in the beginning of the Permian, a heat flow pulse was accompanied by magmatic intrusions and volcanic extrusions. The existence of a net of graben striking orthogonal to the basin axis has been found. According to the model, the increase in heat flow has elevated the Curie depth by about 2.5 km – the metamorphosis boundary was shifted upwards, resulting in a reduction of the affected rock volume by 10%, and subsidence of the overlying surface above by 250 m. The depression was filled by sediments and acted as an additional load on the crust. This starts a positive feedback cycle, as additional greenschist facies rocks are transformed to amphibolite facies. At the level of the Moho ( $700 \text{ }^\circ\text{C}$ ) the rocks could also be affected, due to transformation from amphibolite facies to granulite facies, resulting in a further volume reduction of 10%, and a density increase from  $3000 \text{ kg/m}^3$  to  $3300 \text{ kg/m}^3$ . The granulite facies rocks could be either part of the lower crust or of the upper mantle.

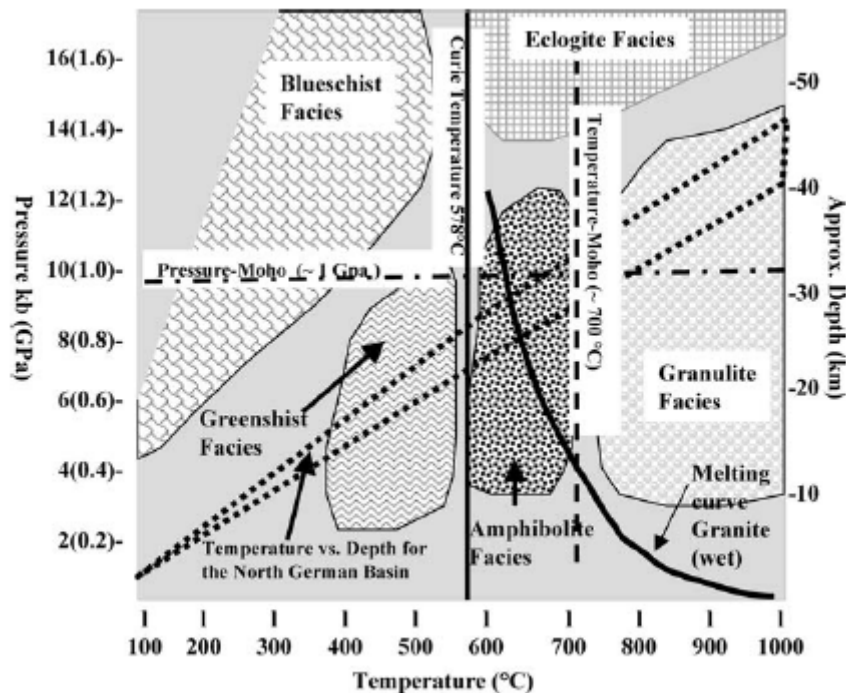


**Figure 1.1** Pressure-temperature diagram for some important metamorphic facies (after Yardley, 1989). Also shown is the temperature distribution of the North German Basin (Brink, 2005).

## 2 AGES AND GEOMETRY OF THE WEST SIBERIAN BASIN

The West Siberian Basin (WSB) is one of the largest intracratonic basins of the world, with an areal extent of approximately  $3.2 \times 10^6$  km<sup>2</sup> (corresponding to the basin outline reported in Fig. 2.1). Published values of the area vary according to the adjoining basins that have been included (e.g. Vyssotski et al. 2006). The basement of the West Siberian Basin consists of Baikalian (Late Precambrian), Caledonian (Cambrian-Silurian) and Variscan (Silurian-Permian) fold systems. A graben system limits the northern part of the basin (Pur-Taz region and Kara Sea). Late Permian evolution is associated with the Siberian flood basalts and intrusives and the basalts appear to cover the entire basin (Vyssotski et al. 2006). The age of the flood basalts is about 250 Ma, with an extrusion time of less than 1 Ma. The flood basalts within the basin are partly within grabens generated by the rifting, but are also present across intervening basement highs, especially in the north (Surkov 2002).

The graben-rift structures have been mapped by Surkov et al. (1982; 1993) mainly by the consideration of gravity and magnetic fields. The criterion for identifying a rift is that of a narrow and elongated axial positive gravity and magnetic anomaly. Other geophysical data that are sought for are: subsidence of the basement as revealed from seismic data, the elevated Moho boundary, low upper mantle refraction velocities, heat flow increases, and the mineral composition of the rift complex (Pavlov 1995). The main graben-rifts that have been proposed (after Pavlov 1995) are: Koltogory-Urengoi, Khudosei, Khudottei, Agan, Ust'Tym and Chuzik. Pavlov (1995) questions the fact that the structures are graben-rifts due to the fact that he does not find the above mentioned criterion to be fulfilled. This standpoint has not been confirmed or acknowledged by later authors. The cited graben-rift structures can be seen in Figure 2.1.

The volcanic eruption that created the flood-basalts was followed by basin-wide subsidence, bringing the basalts down to a depth of 6400 m. It is interesting to note that the flood basalts on the East Siberian Platform remained superficial, pointing to a different buoyancy between the West Siberian Basin and the East Siberian Platform. The post-volcanic stratigraphic section has been analysed by Vyssotski et al. (2006) and covers the Mesozoic to Cenozoic. The deepest well in the basin, SG6 (> 7 km) (Pavlenkova et al. 2002) does not constrain the lower part of the entire sediment package, which reaches 15 km (Pavlenkova et al. 2002). In 2004, 7% of the world's oil production originated from the basin, almost entirely from Jurassic and Cretaceous clastic rocks deposited during the post-rift thermal subsidence phase

of the basin (Vyssotski et al. 2006). Allen et al. (2006) present a rift kinematics of the basin and adjacent areas for the Late Permian - Early Triassic interval, based on the pattern of magnetic anomalies, existing fault maps and recent geochronological data. From the magnetic anomalies they observe the north-south extension of major grabens, but also find grabens with NE-SW orientation, implying a component of NW-SE extension. They suggest that the West Siberian rifting occurred during regional right-lateral oblique extension in the Late Permian-Early Triassic. They furthermore propose a triple junction in the northern part of the basin formed by the ENE-WSW trends in the Yenisey-Khatanga Trough, the NW-SE trending magnetic anomalies crossing the Yamal Peninsula into the Kara Sea, and the north-south trends (e.g. Koltogor-Urengoy, Khudotey and Khudosey grabens), referring also to previous works (Aplonov 1995; Schissel and Smail 2001). Schissel and Smail (2001) attribute the triple junction to the impact of a mantle plume. Consistent with this idea would be the observation that the greatest post-rift subsidence and sedimentation has taken place in this part of the basin (Petersen and Clarke 1991), and that the area has been ascribed to be the focus of the basaltic magmatism (Surkov 2002).

Critical views (e.g. Czamanske et al. 1998) to the existence of a mantle plume argue that, unlike many other flood basalt provinces, there is no obvious succeeding plume 'trail' leading to a presently active hotspot. It is unclear therefore whether any form of mantle hotspot persisted after the formation of the traps. Saunders et al. (2005) come to the conclusion that uplift of the northern part of the nascent West Siberian Basin began during the Permian, maybe accompanied by rifting. Little or no uplift is predicted for the Siberian Craton. The authors suggest further that the main site of magma generation was located primarily in the northern basin (Khudosey and Urengoy rifts) and that the magma source was common to the flood basalts on the Siberian Craton and in the West Siberian Basin. The magma travelled onto the craton either across the land surface and/or through the crust as dykes or sills. The authors propose that following the main period of continental flood basalt formation, the locus of magmatism migrated northwards to what is now the Taimyr Peninsula, and then onto the Barents Shelf. The West Siberian Basin then underwent thermal subsidence (Saunders et al. 2005).



Name of basin, Cratons involved	Lat, min	Lat, max	Long, min	Long, max
Siberian traps	50	72	90	110
West Siberian Basin	50	72	58	90

**Table 2.1** *The geographic windows for the West Siberian Basin and adjoining Siberian traps*

East Barents Basins	Ordovician to Cenozoic Upper Permian-Triassic magmatic bodies	A=0.4 10 <sup>6</sup> km <sup>2</sup> D < 20 km	Gramberg et al. (1999)
West Siberian Basin	Triassic to Cenozoic sediments. Permian–Triassic basalts (250 Ma) overlying possible Permian continental deposits.	A=3.2 10 <sup>6</sup> km <sup>2</sup> D < 15 km	Vyssotski et al. (2006) Statoil basement map
Tarim Basin (area based on sediment thickness model, incl. Qaidam Basin)	Proterozoic-Quaternary Permian basalt layer.	A=1.1 10 <sup>6</sup> km <sup>2</sup> D < 15 km	Chen and Shin (2003) Lithospheric Dynamic Atlas of China (1989)

**Table 2.2** *Age of magmatism, areal extension (A) and thickness (D) of the West Siberian, East Barents and Tarim Basin.*

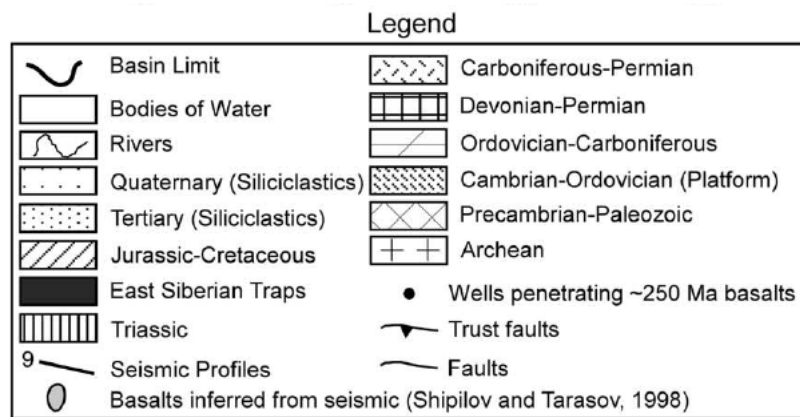
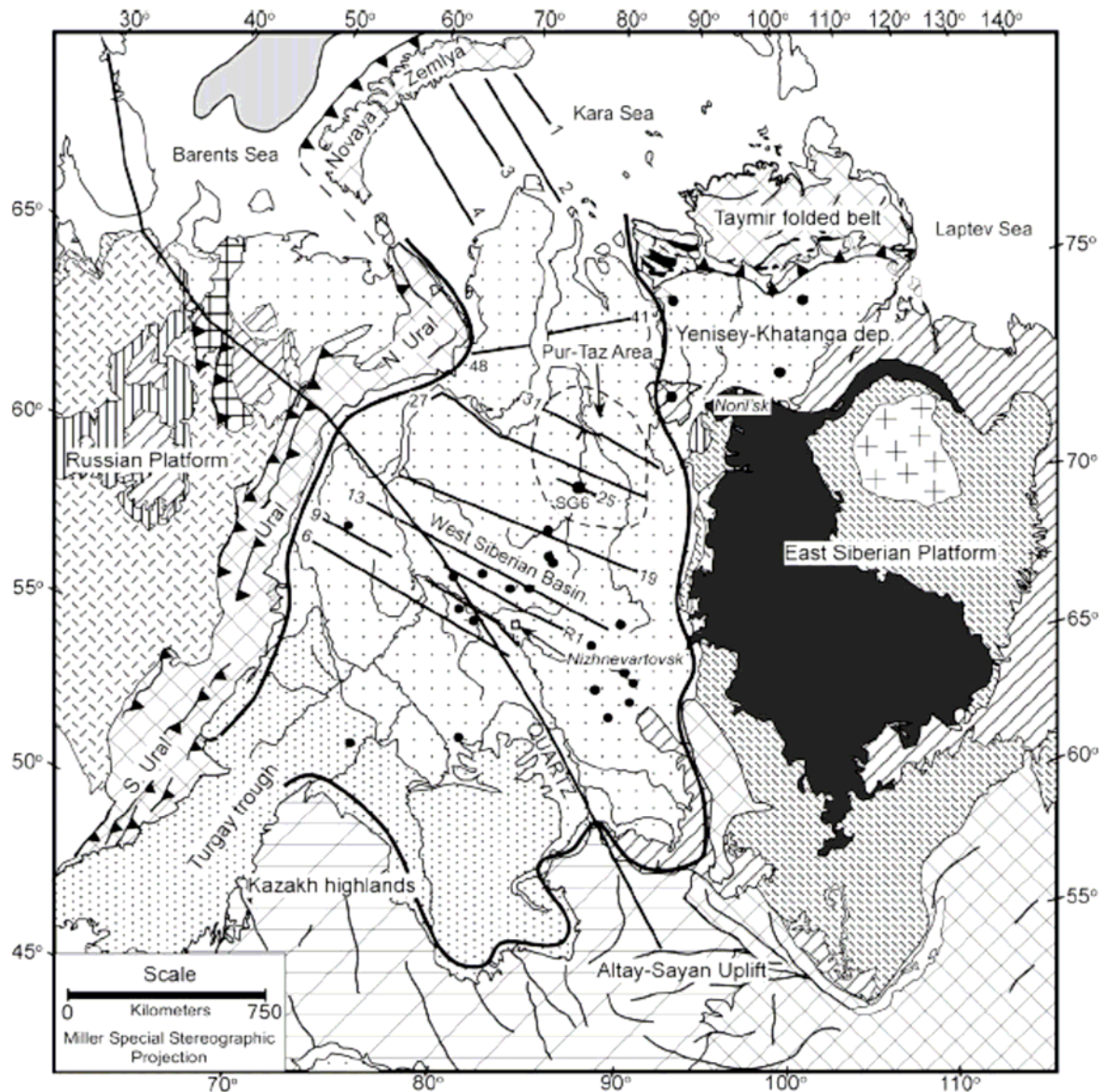


**Figure 2.1** West Siberian Basin: basin geometry (Vyssotski et al. 2006). The basin is outlined with the bold black line; the northward extent of the basin is not defined according to Vyssotski et al. (2006).

### **3 DATABASES USED IN THE STUDY- PRESENT STAGE AND UPCOMING DATA**

We describe in the following chapter the data sets that we used for our study: geoid and gravity field, the digital terrain model, models for the thickness and depth of sediments, models for the crustal thickness variation, and models for the location of the basalt layer. We have made an extensive research on available data, which included publications and digitally available data. Partly, the data had to be digitized by hand from the relevant publications.

#### **3.1 Gravity and topography data**

Our analysis had to rely on publicly available regional data, as detail local data have not yet been available. The digital topography consists of the 1-km grid GLOBE (Global Land One-km Base Elevation) released by the National Geophysical Data Center in Boulder, CO (NGDC). The topography is indispensable for calculating the isostatic loading and for correcting the gravity data for the effect of topography (see Fig. 3.1). Gravity field data are available at a spatial resolution of  $0.5^{\circ} \times 0.5^{\circ}$  using the recent GRACE (Gravity Recovery and Climate Experiment) satellite data integrated with terrestrial gravity measurements.

One model is the GGM02C model, which has been obtained from the combination of the satellite derived gravity field and terrestrial gravity data. In the harmonic expansion, the coefficients up to degree and order 120 are purely from the satellite measurements, the degrees 120 to 200 have been obtained by a combination of the purely satellite gravity data and the terrestrial data, in the form distilled in the EGM96 harmonic expansion (Tapley et al. 2005). The combined field, from order up to 200 is freely available from the GRACE homepage (<http://www.csr.utexas.edu/grace/gravity/>) and is termed GGM02C. Details on the construction of the field are found in Tapley et al. (2005).

In general, the improvement of lower harmonics of the GGM02C with respect to the EGM96 model is very important not only in geoid computation but also in the Moho estimation, since the low harmonics are closely related to deep subsurface structures like the Moho and the deeper interior of the Earth. The improvement of the gravity recovery of the GGM02C is shown in Fig. 3.2, of which the accumulated error at degree 120 is estimated to be only about 1.5 mGal, significantly better than the value of about 4.9 mGal for the EGM96.

We have adopted the solution of the GFZ Potsdam with coefficients of the spherical harmonic expansion up to degree and order 360 (EIGEN-GL04C, Förste et al. 2006). This solution is preferred to the GGM02 solution, due to the fact that the coefficients greater than  $n=120$  for the GGM02 solution have been taken from the EGM96 model, whereas the same coefficients of the EIGEN-GL04C solution have been recalculated. We use this expansion for obtaining the gravity field as well as the geoid. By end of the year 2007 a new gravity field shall be released, with spherical harmonic coefficients up to degree and order 1240, allowing a 3-fold resolution in space.

### **3.2 Topographic correction of gravity and geoid fields**

The combined satellite and terrestrial gravity fields must be corrected for the topography in order to obtain the Bouguer anomaly and the terrain corrected geoid, the latter the counterpart of the Bouguer anomaly in the geoid field. It is useful to correct the data for the topography, as then the crustal masses are more evident in the maps. We use the DEM mentioned above for the near field reduction, and have computed a coarse grid ( $0.1^\circ$  resolution) from the above DEM for the far field reduction. The computation is based on two digital elevation models, a detailed and a coarse one, which is used in the inner ( $<10$  km) and outer zones (10 to 167 km), respectively. Calculations are computed for a spherical Earth, by using the approximation with prisms, following the procedure proposed by Forsberg (1984), using own software and the GRAVSOFIT package (Tscherning et al. 1992).

### **3.3 Moho depth**

We have considered the use of the publicly available Moho depth model and sediment thickness model of the global crust 2.0 (Bassin et al. 2000; CRUST 2.0, 2006). The Moho is available at the resolution of  $2^\circ \times 2^\circ$ , which is too low for our purposes. It should be noted, that the results of Kaban et al. (2003), who arrived at the conclusion that cratonic basins are underlain by low density mantle, including the West Siberian Basin, must be questioned. A Moho depth map for the Western Siberian Basin is found in Vyssotski et al. (2006) and in Artryushkov and Baer (1986). The sediments in the same model are available at the resolution of  $1^\circ \times 1^\circ$ , which also is a rather crude estimate for our study. As a more viable reference we have considered and digitised the Moho map (Fig. 3.4) reported in Vyssotski et al. (2006), which is based on Kovylin (1985). A very similar Moho depth map is reported in Artyushkov

and Baer (1986), based on Karus et al. (1984). The Moho below the basin is between 36 and 40 km deep, and deepens to 48 km towards the Urals and towards the East Siberia Platform to the east. Shallow values of the Moho are found below the Kara Sea. One problem consists in the fact, that we cannot estimate the reliability of the Moho depth. For an improved study of the basin, it would be essential to obtain more information on how the Moho map was constructed, where the values are best constrained, e.g. by seismic investigations, and what the uncertainty on the published values are.

### **3.4 Basement depth and sediment layer**

For the West Siberian Basin a sediment thickness model was provided by Statoil with a spatial resolution of 5'x5' on a spatial window that covers the entire West Siberian Basin. Figure 3.5 shows the sediment thickness for the West Siberian Basin. The sediment thickness model describes the entire sediment package, which includes the pre- and post-Late Permian/Triassic extensive basalt layer. The thickest sediment deposits reach the thickness of over 15 km: these are found at long. 77.85°, lat. 67.33° (along profile 31) and farther to the north at long. 77.85°, lat. 67.33°. The sediments propagate eastwards into the Yenisey-Khatanga deposits continuously, without the presence of a dividing high. In the southern half the basin widens, but the deepest part (thickness >5000 m) is elongated and relatively narrow, indicating smaller characteristic wavelengths. In the southern part of the basin we find a succession of NNW-SSE linear-oriented deepening structures in the basement.

We have digitised the six east-west trending seismic profiles published in Vyssotski et al. (2006), ranging from latitude 60.48° to latitude 70.81°, and converted the TWT times into sediment thickness by the conversion relations described later in Chapter 4. We depict that horizon in the profiles, which has been termed the acoustic basement, and has been attributed to the separation between the pre-volcanic Permian sequence and the post-volcanic Middle-Jurassic sequence. Over some segments of the profiles this horizon corresponds to the ~250 Ma flood basalt event (Tunguska basalts) capping the Permian continental deposits (basin-wide) and the rift sequence (north-northeast only) (Vyssotski et al. 2006).

We compare the total sediment thickness (red) with the depth of the acoustic basement (blue) in the southern (Fig. 3.6a) and northern (Fig. 3.6b) sector of the West Siberian Basin. Starting in the south, the two horizons differ by maximum 2000 m at the most. Moving northwards,

the basement depth increases drastically, whereas the Permian horizon deepens more moderately. At latitude 64°, the basement divides into two lows that we interpret as the Khudottey graben to the west and the Koltogor-Urengoy graben to the east. At latitude 67.5°, the Profile 31 cuts through three parallel graben-structures, where the basement steeply deepens up to 4000 m below the acoustic basement.

It is interesting to notice that the top Perm horizon does not resemble the steep flanks of the underlying basement. When returning to the Moho depth (Fig. 3.4) we notice that it reaches deeper values close to 42 km in areas with supposed rifts below the sedimentary rocks. The sediment thickness from the Statoil database is in turn always deeper than the acoustic basement and should correspond to the total sediment thickness down to the Palaeozoic basement (see Fig. 3.6 a,b). It is interesting to note, that the wide-spread basalt layer in some areas caps a thick presumably Permian sequence, which is up to 6000 m thick.

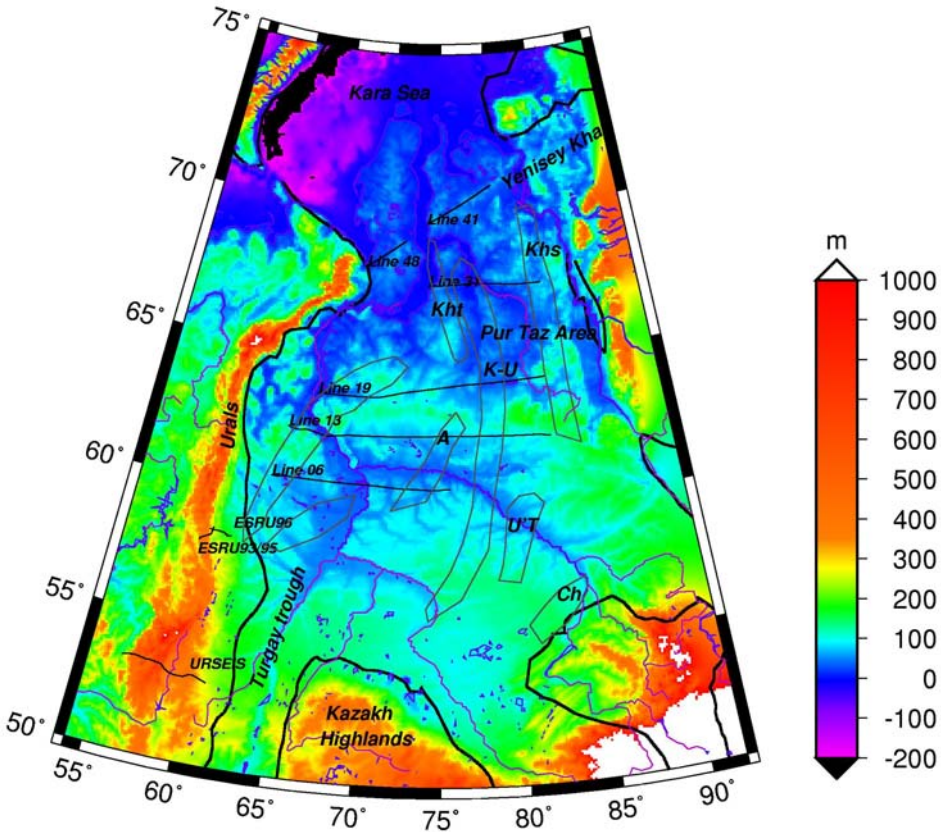


**Figure 3.1** Topography of the West Siberian Basin area. Coastline and rivers (purple), basin outline (bold black). Also shown are regional seismic profiles (thin black) used later and the proposed graben-rift structures (grey; after Pavlov, 1995). Names of graben-rifts: K-U, Koltogory-Urengoi; Khs, Khudosei; Kht, Khudottei; A, Agan; U'T, Ust' Tym; Ch, Chuzik.

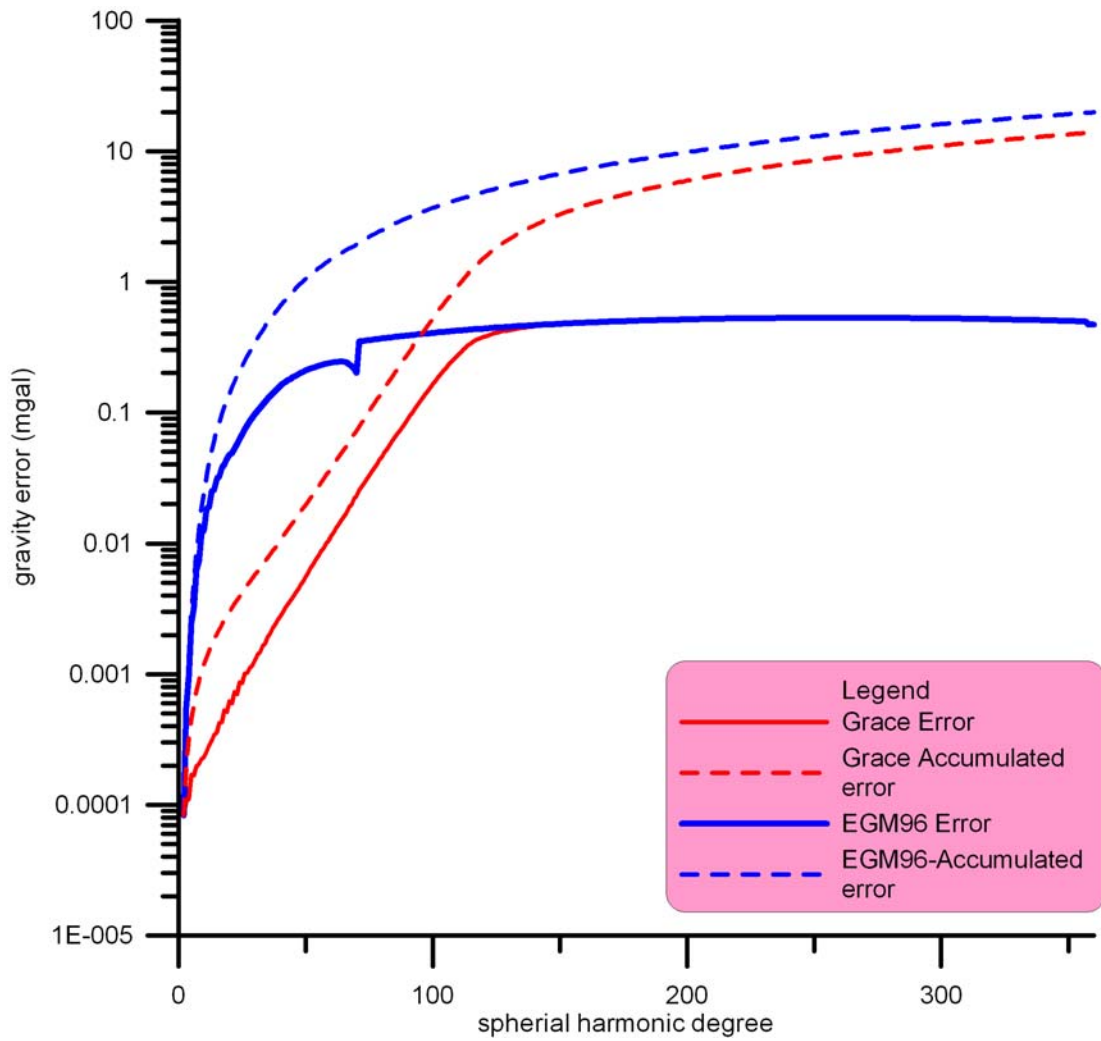


**Figure 3.2** Amplitude of gravity errors of the GGM02C and the EGM96; computed from the standard deviation coefficients of the models.

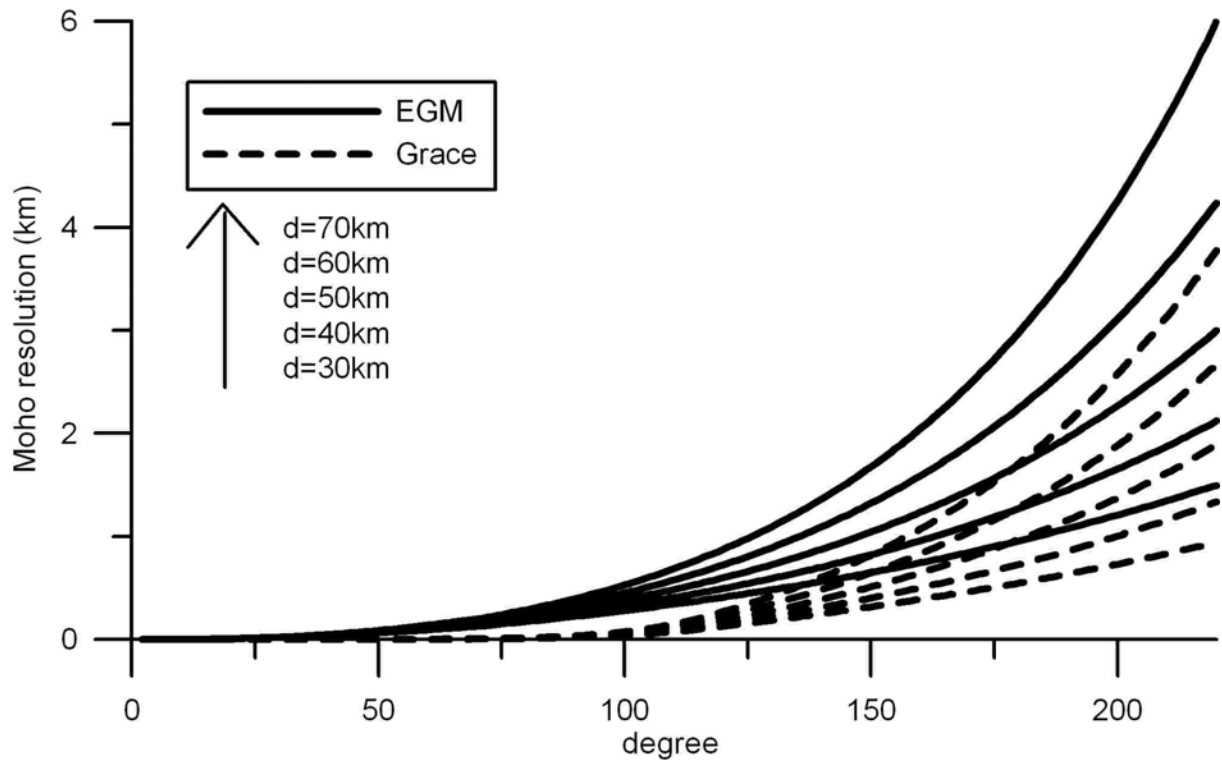


**Figure 3.3** Resolution power of the GRACE gravity field in the estimate of Moho undulations. Set of curves pertain to average Moho-depths between 30 and 70 km. The curves were obtained by inverting the accumulated error curve for GRACE and EGM96 (Figure 3.2). Density contrast at the Moho boundary:  $500 \text{ kg/m}^3$ . The resolution is even better for smaller densities.



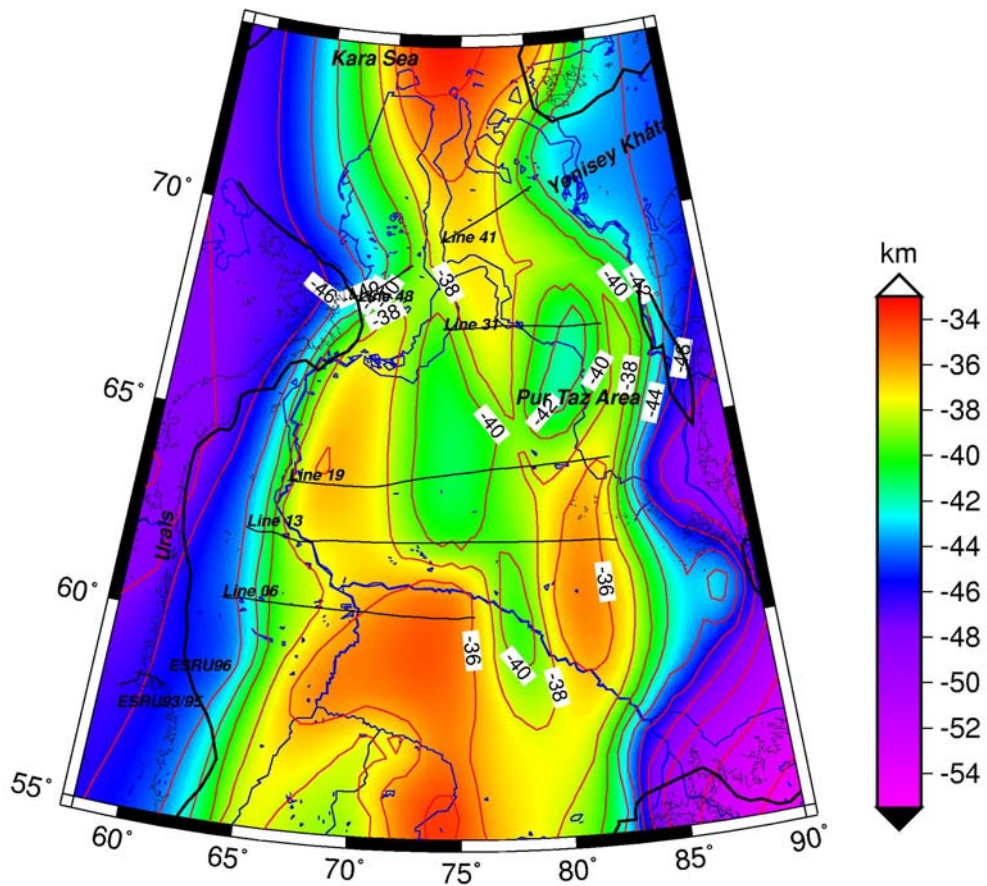


**Figure 3.4** Moho depth for the West Siberian Basin area, digitised from Vyssotski *et al.* (2006) based on an older work by Kovylin (1985). Basin outline (heavy black) and 200 m topography isohypse (light black). Black lines show regional seismic profiles. Coastline and rivers (blue).

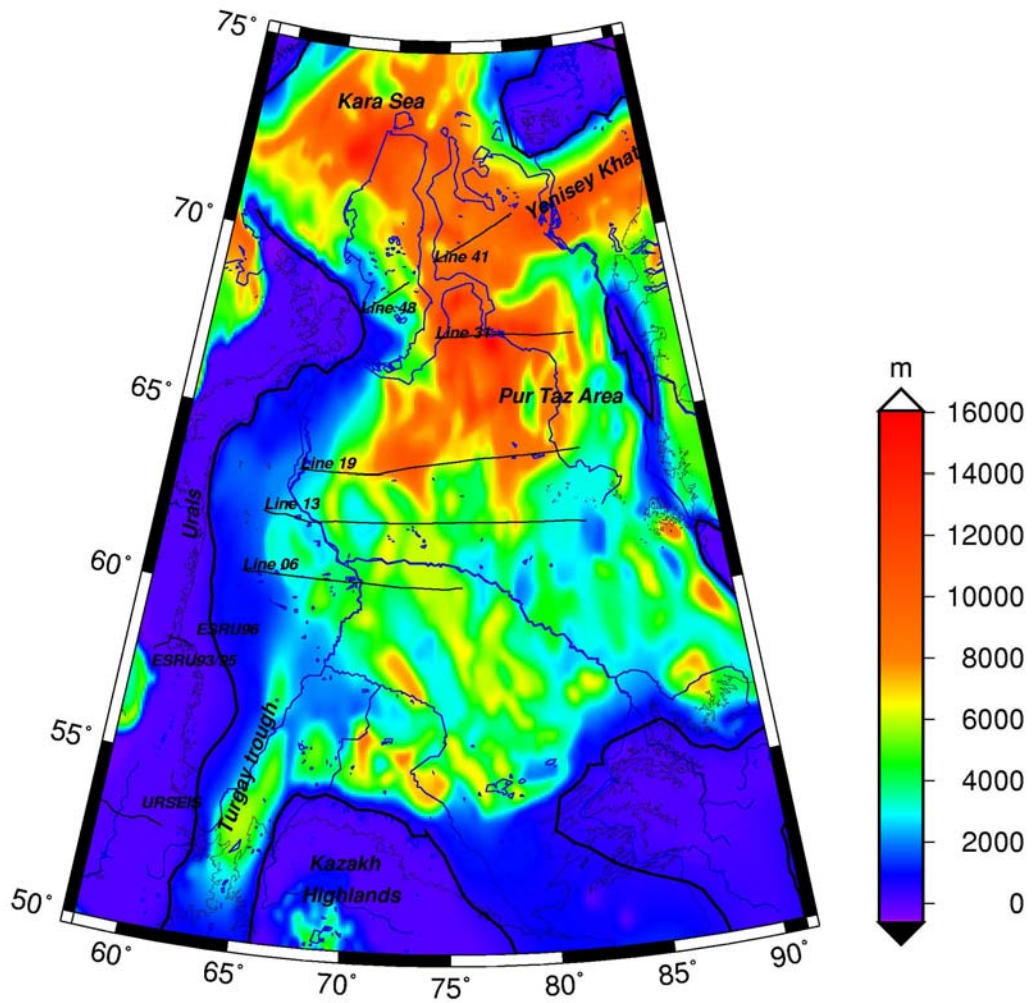


**Figure 3.5** Sediment thickness map from the Statoil database. Basin outline (bold black) traced along the 500 m isopach line. Thin black lines show regional seismic profiles.

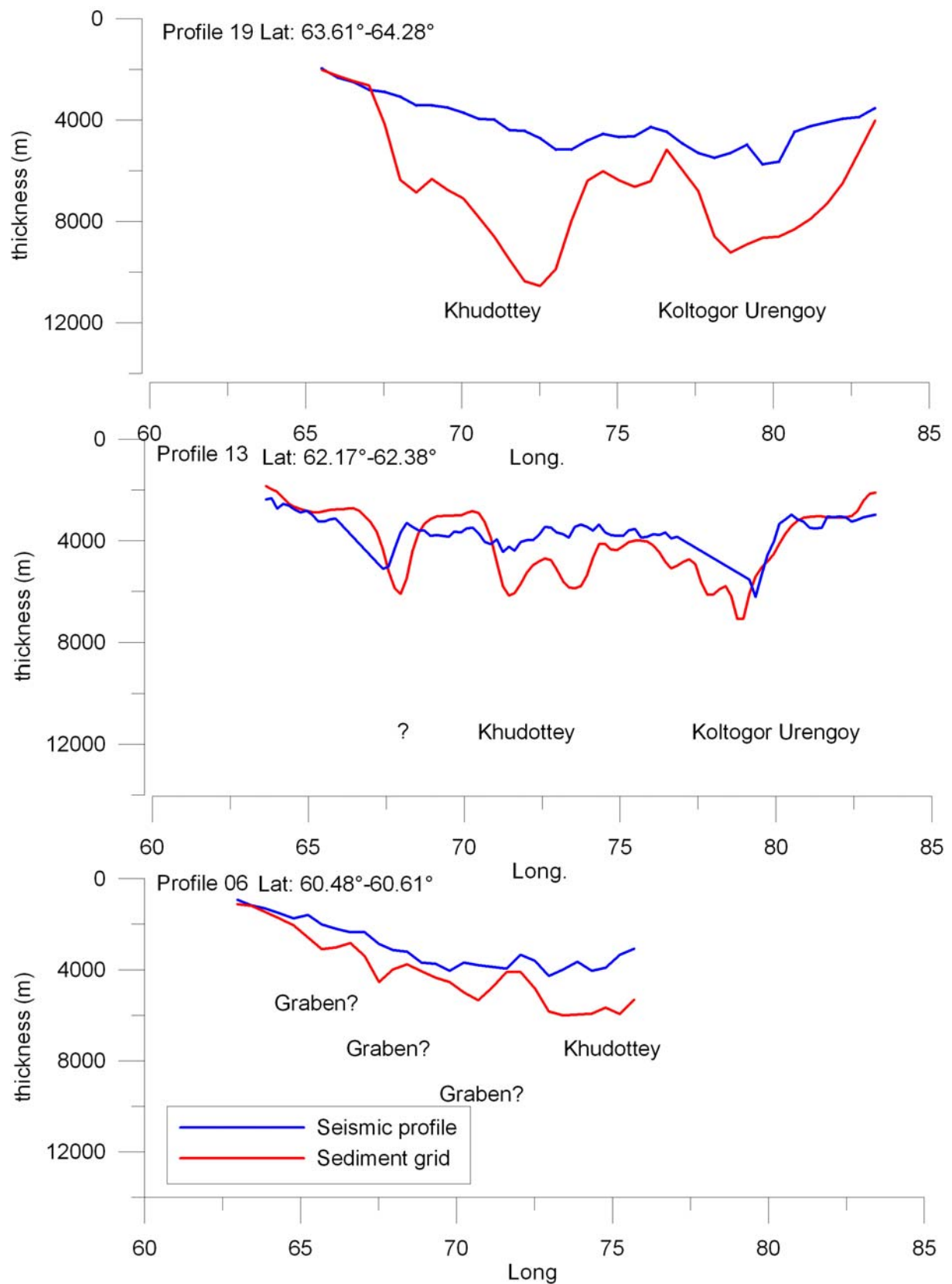


**Figure 3.6 a** Southern West Siberian Basin sector: Total sediment thickness (red) from Statoil database and horizon separating the pre-volcanic and the post-volcanic sedimentary rocks (blue), digitised from Vyssotski et al. (2006).

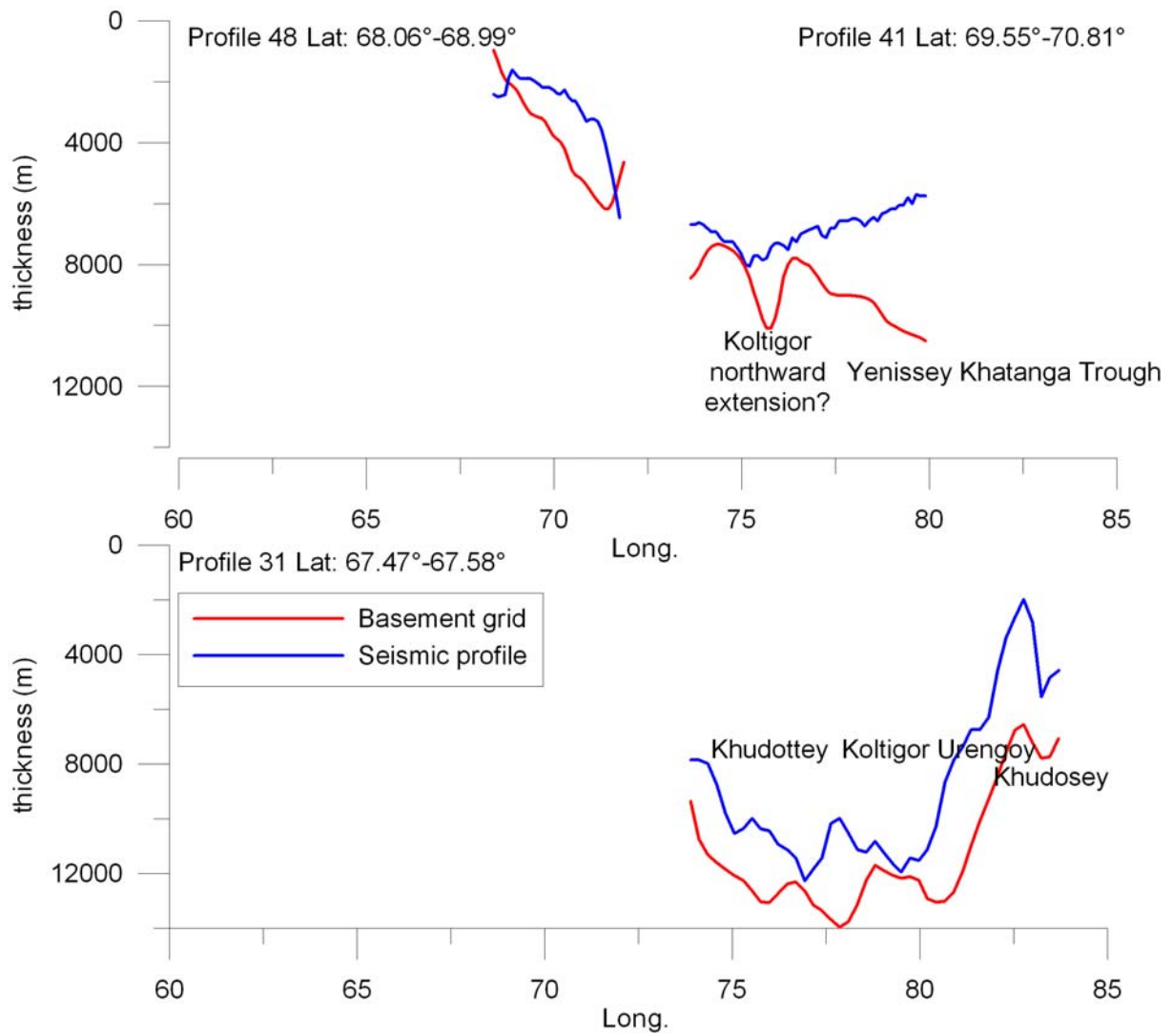


**Figure 3.6b** Northern West Siberian Basin sector: Total sediment thickness (red) from Statoil database and horizon separating the pre-volcanic and the post-volcanic sedimentary rocks (blue), digitised from Vyssotski et al. (2006).

## 4 TWO-WAY-TRAVELTIME TO DEPTH CONVERSION.

Necessary input to our study is the depths to the basement and to the basalt layer. We obtain this information from published seismic lines. We use six of the E-W running regional seismic profiles reported in Vyssotski et al. (2006), the reflection horizons being given as two-way-traveltime (TWT) in seconds. This requires the conversion to depth, in units of meters. Along the seismic lines the depth to the horizons are calibrated by the use of boreholes. We use this information to determine an empirical TWT-depth function, which we may use to extrapolate the digitised TWT values of each horizon to the correct depth value. We also determine an empirical velocity-depth relationship, which will be used later for the modelling.

### 4.1 Empirical TWT-depth and velocity-depth function

As discussed above, the paper of Vyssotski et al. (2006) presents a series of profiles across the West Siberian Basin. They report the calibrated TWT (two way travel times) for some horizons. In Fig. 4.1 the TWT is plotted vs. depth for the Profiles 6 and 19. The TWT of Profile 6 reveals to have a strong deviation at shallow depths from the values found in Profile 19 and from a quite regular depth variation. We must now choose a function with which to fit the data.

We have tested different analytical curves to model the depth versus TWT values. We find that the exponential equation gives a reasonable fit to the data. Fitting the observed data of depth and TWT to an exponential function derives the following relation:

$$d = 387.3 \left( e^{0.893TWT} \right) \quad (4.1)$$

For the TWT to depth conversion of the profiles discussed in Par. 3, we have used this exponential function.

A second problem regards using the TWT to depth function to obtain some information on the velocity of the strata. Considering the near to vertical reflection, the TWT of a wave reflected at a horizon with depth  $d$  is equal to:

$$TWT = 2 \int_0^d \frac{1}{v(z)} dz \quad (4.2)$$

where  $v(z)$  is the velocity as a function of depth. Assuming a linear velocity increase with depth:

$$v(z) = \beta + \gamma z \quad (4.3)$$

resulting in:

$$TWT = 2 \int_0^d \frac{1}{\beta + \gamma z} dz = 2 \frac{1}{\gamma} [\ln(\beta + \gamma z)]_0^d = 2 \frac{1}{\gamma} ([\ln(\beta + \gamma d) - \ln(\beta)]) \quad (4.4)$$

and:

$$TWT = \frac{2}{\gamma} \ln \left( 1 + \frac{\gamma}{\beta} d \right) \quad (4.5)$$

We therefore fit the values of TWT as a function of depth for Profiles 6 and 19 to the above function. The function results to be, with  $d$  the depth in m and TWT in seconds:

$$TWT = -2/0.88 * \ln( 1 + \text{depth} / 1724.44 ) \quad (4.6)$$

Equating with the above relation it results, that

$$\begin{aligned} \beta &= 1575.5 \\ \gamma &= 0.88 \end{aligned}$$

This implies:

$$v(z) = (1575.5 + 0.88 z) \quad (4.7)$$

The velocity is thus of 1.6 km/s near the surface, increasing linearly with depth by 0.88 km/s every km.

The knowledge of the depth-dependency of velocity provides some indication on which densities should be expected for the sediments with depth, by applying an empirical velocity-density relation. We compare the a-priori density function we have previously used, with a linear density increase from 2275 kg/m<sup>3</sup> to 2700 kg/m<sup>3</sup> between 0 and 6 km sediment-thickness, and a constant density below (2700 kg/m<sup>3</sup>) with the densities calculated from the velocity depth relation. This comparison is a check on the consistency of the inferred depth increase of velocity and the assumed density increase with depth. As uncertainties exist regarding the velocity-density relationship, we adopt three relations, the well known Nafe-Drake curve (Ludwig et al., 1970; Jones, 1999), Gardner's rule (Gardner et al. 1974), and Hamilton's relations (Larsen et al. 1994), all three valid for sediments. The results are shown in Fig. 4.2, and it can be seen that the velocity model and the density model are consistent with the three velocity-density relations.

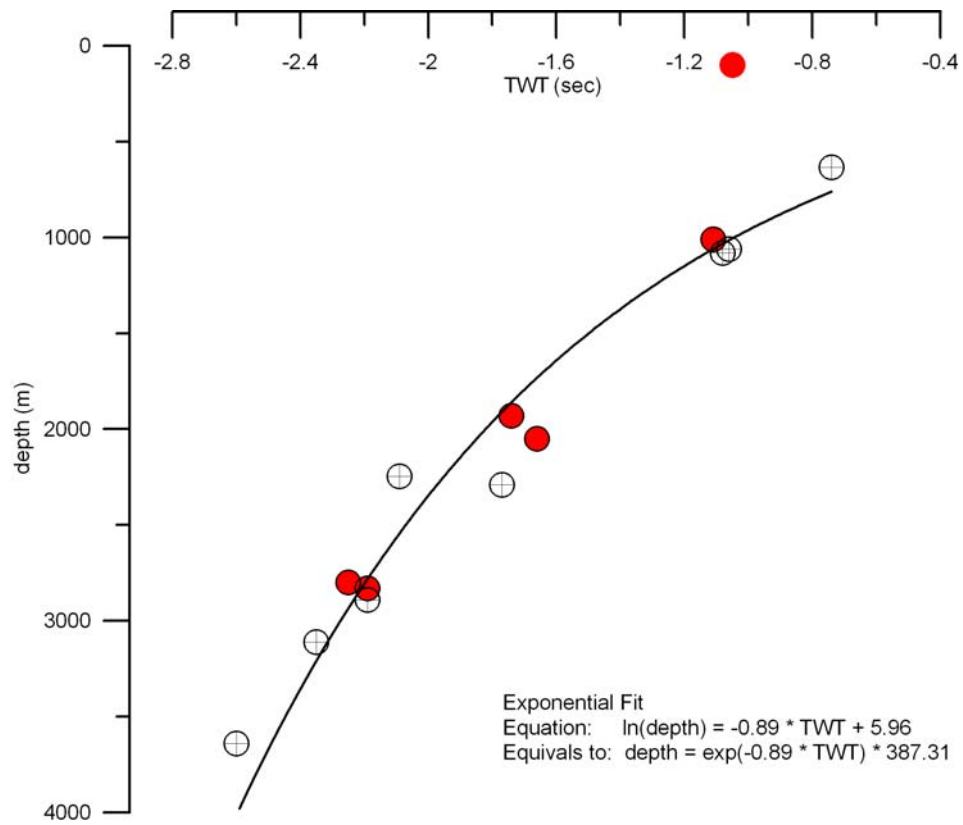


**Figure 4.1** Experimental depth dependency of the TWT for regional seismic profiles 06 (red dots) and 19 (discs with crosses). The interpolated curve is used to convert the horizons given in units of TWT to depths.

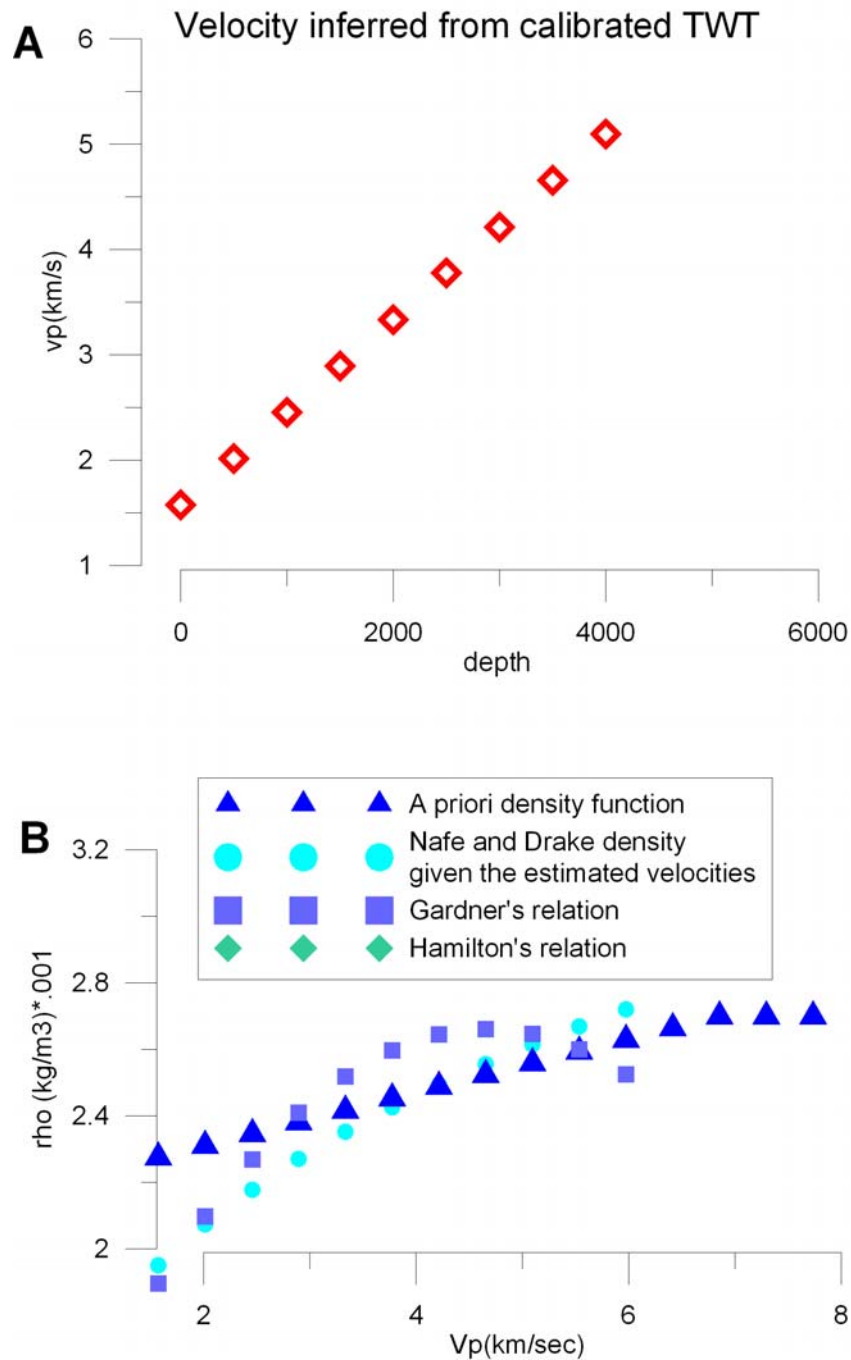


**Figure 4.2** a) Velocity of sediments in function of depth. The relation was found from the analysis of the TWT. b) Comparison of the a-priori depth-dependent linear density increase with the density corresponding to the above velocities. Different relations were used for calculating the relation of density to velocity (Nafe-Drake (Ludwig et al., 1970; Jones, 1999), Gardner's rule (Gardner et al. 1974), and Hamilton's relations (Larsen et al. 1994).



## 5 GRAVITY AND GEOID FIELDS

In the following chapter we discuss the observed gravity and geoid fields and determine to what extent the observed fields comply with the knowledge on the crust and lithosphere. The results of this chapter allow recognizing differences in the terranes constituting the West Siberian Basin.

### 5.1 Gravity anomaly and Bouguer anomaly

In Fig. 5.1 the gravity anomaly for the entire West Siberian Basin, the Urals, and the Kara Sea is shown. For better orientation we have included the regional seismic profiles discussed in Ch. 3.3, and the profiles of the Europrobe seismic reflection profile across the eastern middle Urals and the West Siberian Basin (ESRU) (Friberg et al. 2000) and the URSEIS 95 seismic experiment (e.g. Döring and Götze, 1999). The gravity anomaly over the central area of the West Siberian Basin is between -5 and -25 mGal (Fig. 5.1). Three linear highs emerge clearly in the northern part of the basin, and are probably associated with structures in the Paleozoic basement, as can be seen by comparing the Profiles 27, 31 and 19 of Vyssotski et al. (2006). In particular, we may tentatively interpret the linear positive anomalies with the graben structures proposed by Allen et al. (2006), which are the Khudotey (west), the Koltogor Urengoy (central) and the Khudosey (east) graben. We have added the inferred graben-rift structures (Pavlov, 1995) to the map. The basin is bounded by positive gravity anomalies: the Urals (+ 60 mGal), the Kazakh highlands to the south (20 mGal) and the East Siberian Platform to the east. The Bouguer field (Fig. 5.2) has very similar features to the gravity anomaly in the West Siberian Basin: the basin has generally negative anomalies, oscillating around -15 mGal. The Urals and the three positive linear features noticed in the gravity anomalies remain. There is though a general decrease of the anomalies towards SE, leading to the Kazakh high-planes and the Altai ranges (compare with topography map, Fig. 3.1). The decrease is surely due to crustal thickening as an isostatic response to the increase in topography. The Urals do not show the decrease in Bouguer gravity, which is evidence that the crustal thickness does not respond isostatically to the Ural range.

## **5.2 Geoid and terrain corrected geoid**

Due to the different distance dependency of the gravity potential, the geoid undulations average the anomalies over a greater area and are representative generally of deeper lying structures with respect to the gravity field. We consider the geoid undulations reduced from the longest wavelength variations. We have systematically subtracted the geoid field up to degree and order 10 in the spherical harmonic expansion in order to obtain a field representative of crust and upper mantle structures. This reduction corresponds to subtracting the components of the field with wavelength greater than 2000 km at mid-latitudes. We denominate the resulting field as residual geoid in the remainder. The terrain corrected geoid is the analogue to the Bouguer gravity field, and has been reduced from the effect of topographic masses.

Considering the geoid residual (Fig. 5.3), the basin lies in a concentric geoid low. The central part of the basin has a general decrease in the geoid height with higher values surrounding the basin, the Urals show for example a broad geoid high. The terrain corrected geoid (Fig. 5.4) is interesting, as it repeats the northern positive linear features, observed in the gravity field, indicating that these are major features affecting not only the basement, but probably also the lower crust. The deepest part of the basin lies in a geoid minimum (A in Fig. 5.4). The two relative geoid highs (B & C in Fig. 5.4) correspond to the two areas with shallower basement. Only detailed modelling can though give more quantitative and definitive results.

## **5.3 Sediment gravity effect**

The Bouguer anomaly represents the gravity field produced by the crustal column, excluding the topography. We now need to estimate the gravity field produced by the sediment layer, with the scope of correcting the Bouguer field for this known unit. We use the entire sediment package that contains both post- and pre- basalt flow layers, using the isopach map discussed in Ch. 3.3.

The constraints on the sediment-depth variation are given along the six profiles we have digitised from Vyssotski et al. 2006. For modelling, we take into account the compaction of sediments, leading to a density increase with depth. The model corresponds to a linear density

increase from 2.275 to 2700 kg/m<sup>3</sup> up to a depth of 6 km, and constant density of 2700 kg/m<sup>3</sup> below (Fig. 5.5a), adopting the relation discussed in paragraph 4, that velocity increases linearly with depth. The gravity effect of the sediments is near to -50 mGal over large part of the basin, and in the Kara Sea, with maximal values reaching -70 mGal.

We choose model 1 for the further work, but it should be borne in mind that there are some uncertainties. The sediment corrected Bouguer field is shown in Fig. 5.6. The sediment correction shifts the Bouguer values upward: the maximal residual values are found towards the Kara Sea and the Urengoy-Khatanga trough. The Pur-Taz area emerges as a relative high. From here two linear gravity highs protrude southwards, which could resemble the Urengoy and the Khudosey Graben structures. A secondary gravity high is found east of the Urals in the basin, and is covered by the western extremes of the seismic lines 19, 13, and 06. The Urals form a pronounced gravity high. The Urals have been studied in detail by the URSEIS (south) and the EUROPROBE seismic investigations for the middle Urals (Friberg et al. 2000). The gravity high of the Urals is well known and has been studied before, explaining it by the combined effect of mafic-ultramafic rocks posed on the surface and high-density rocks at Moho level (Döring et al. 1997; Döring and Götze, 1999) or the effect due to a relict SW dipping subduction (Friberg et al. 2000).

#### **5.4 Gravity effect of crustal thickness variations**

We rely on published maps of the Moho depth to calculate the gravity effect of crustal thickness variations (see Ch. 3.3). We use a standard earth reference model and standard value of 350 kg/m<sup>3</sup> as the density contrast at the Moho. The resulting gravity effect is given in Fig. 5.7. The values vary between -180 mGal (min.) and -30 mGal (max). A different density contrast will linearly affect the gravity field. That means, that a 10% increase in the density contrast results in a 10 % increase of all the gravity values reported in Fig. 5.7. It is interesting to note, that towards the Urals, the crustal thickening is independent from the topography, and commences already well in the basin, eastwards to the topographic increase tied to the Uralide. If the model is correct, the Moho variations seem to be overprinted by buried features, rather than the transition from basin to orogen.

We now proceed to calculate the residual field, i.e. the Bouguer field corrected for sediments and crustal thickness variations (Fig. 5.8). The correction further shifts the gravity values

upward, due to the fact that the Moho is below the standard reference depth. The residual field has its maximal values along the Urals. The linear gravity high correlating with the central Urals is off-centred towards east into the basin, in the northern Urals. This is an interesting feature, as it is probable that the cause of this high gravity signal is found beneath the basin in the northern part of the orogen. Further high values are in the northern part of the basin, where we also have found the maximal sediment thickness. In order to distinguish the features contained in the residual field, we separate smaller wavelengths than 150 km (Fig. 5.9), from that longer wavelengths (Fig. 5.10). Observing the high pass filtered residual (Fig. 5.9), we can now distinguish several features in the basin: an almost symmetric gravity high along the eastern and western border of the basin, where the western high is partly centred on the Urals, and partly spills eastward into the basin. The Pur Taz area is a general high, from which a linear high protrudes southward, and which is identified with the Koltogor-Urengoy and Khudosey grabens. A further linear positive anomaly, and presumably tied to a graben is found to the east of the Urals. This could be the westward extension of the proposed Agan graben. The Kara Sea has small residual anomalies, an indication that the crustal thickness variations and the sediments are sufficient to explain the observed gravity field. The Yenisey-Khatanga Trough features positive residual anomalies.

The low-pass filtered residual (Fig. 5.10) shows entirely positive values that range between 50 and 150 mGal. Two symmetrically disposed positive anomalies are seen also here and they delineate the basin along its eastern and western border: the one to the east lining the transition to the Siberian Platform, the one to the west the Urals. The basin itself is dissected by a NE-SW trending relative gravity high that is about 50 mGal higher than the adjoining part of the basin. This positive gravity zone is coincident with the areas of the inferred graben and rift structures, but cover a broader region. In the northern part of the basin, the Yenisey-Khatanga trough reveals high gravity anomalies as well as the transition to the Kara Sea northwards.

The high residual values demonstrate that the sediment-correction and the correction of the crustal thickness assuming constant crustal density, is insufficient to explain the observations, implying that mass-inhomogeneities other than sediment thickness variations and crustal thickening are present.

## 5.5 Gravity effect of the basalt layer

The areal extent and the thickness of the basalt layer in the West Siberian Basin is known only as a rough estimate. Vyssotski et al. (2002) report a minimal and maximal extent, with a difference of 100%. The recovery of the basalt layer in boreholes (see Fig. 3.1a) demonstrates that the basalt extends over large parts of the West Siberian Basin. For our study it is important to know the gravity contribution of the basalt layer to the gravity field. For this scope we have digitised the information on the presence of the basalts contained in the line drawings of the regional seismic profiles 06, 09, 13, 19, 27, 31, 48 and 41 from the publication of Vyssotski et al. (2006). Profile 48, located northwest to the Pur-Taz area does not report the basalt layer. We interpolate the acoustic basement, which corresponds to the top Perm and the top basalt level onto a regular grid with 15 km spacing. The extent we obtain for both the acoustic basement and the top basalt level is affected by several problems, before it can be taken as a satisfactory representation of reality: the profiles are relatively short and the spacing between them is rather large, for allowing a good 3D representation of the basalt-layer. We may regard the estimate as a first approximation, which in its areal extent is subject to possible major changes (Fig. 5.11). It is nonetheless useful for obtaining a rough idea of the strength of the gravity signal that may be produced by the basalts. From the profiles the basalt layer results to be mostly below 1 km thick, only in the north-eastern part, corresponding to Profiles 27 and 31, in the Pur Taz area, does the basalt layer increase to 2 km thickness. With a contrast density of  $300 \text{ kg/m}^3$  the basalt layer produces a gravity signal that amounts to 16 mGal (see Fig. 5.12). The greatest signal pertains to the Pur Taz area. The uncertainties on the calculated gravity signal are so large, that we do not think a correction of the observed gravity is useful. We will use the estimated value in the discussion, and as a means to evaluate the final uncertainties on our results.

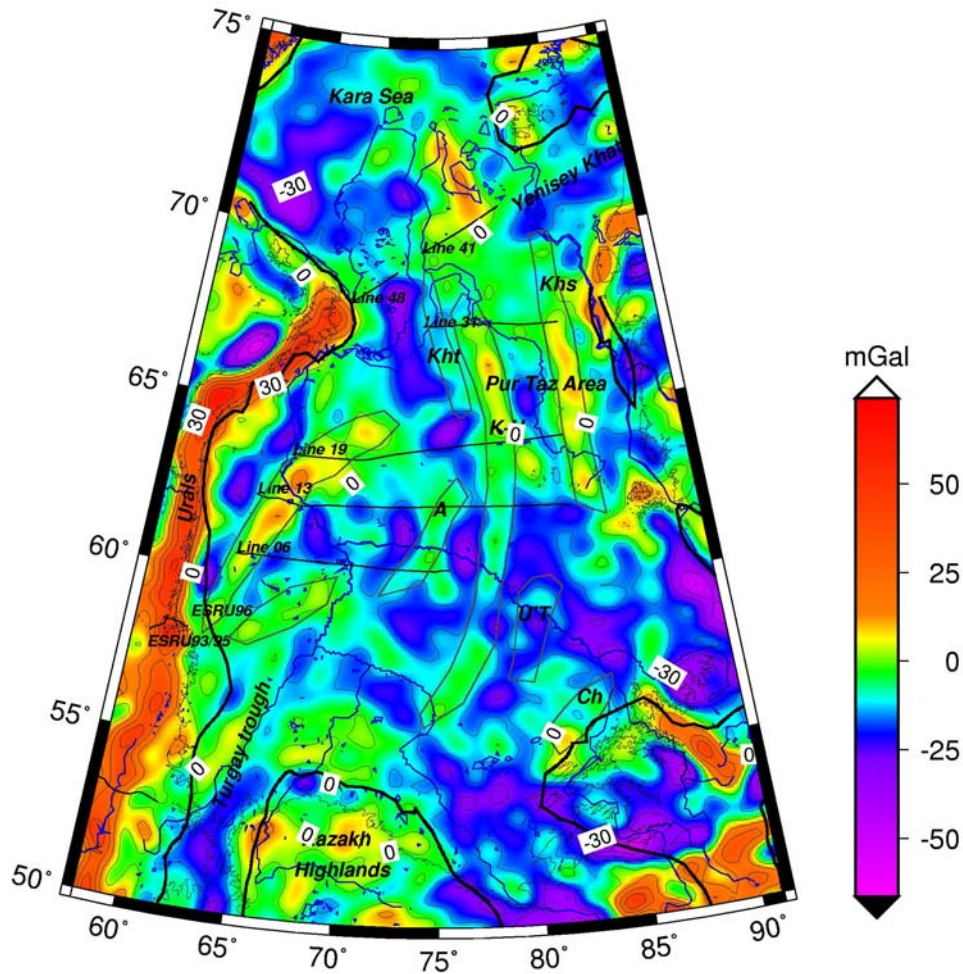


**Figure 5.1** Free-air gravity anomaly ( $\text{mGal} = 10^{-5} \text{ m/s}^2$ ) for the West Siberian Basin area. (Data: EIGEN-GL04C, Förste et al. 2006). Coastline and major rivers in blue. Isoline interval 15 mgal. Basin outline (bold black). Topography 200 m isoline (thin black). Also shown are regional seismic profiles and the proposed graben-rift structures (grey; after Pavlov, 1995). Names of graben-rifts: K-U, Koltogory-Urengoi; Khs, Khudosei; Kht, Khudottei; A, Agan; U'T, Ust' Tym; Ch, Chuzik.

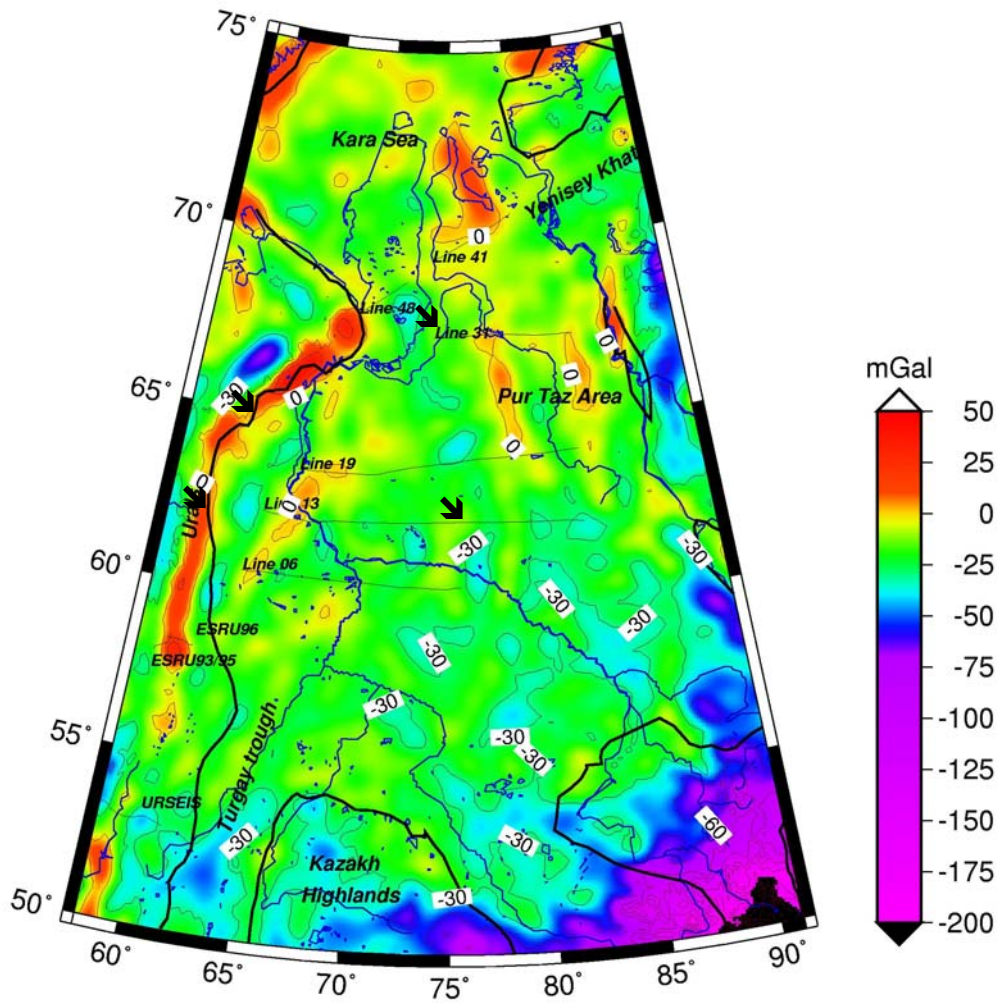


**Figure 5.2** Bouguer gravity anomaly (mGal) for the West Siberian Basin area. (Data: EIGEN-GL04C, Förste et al. 2006). The linear gravity highs are marked by black arrows.

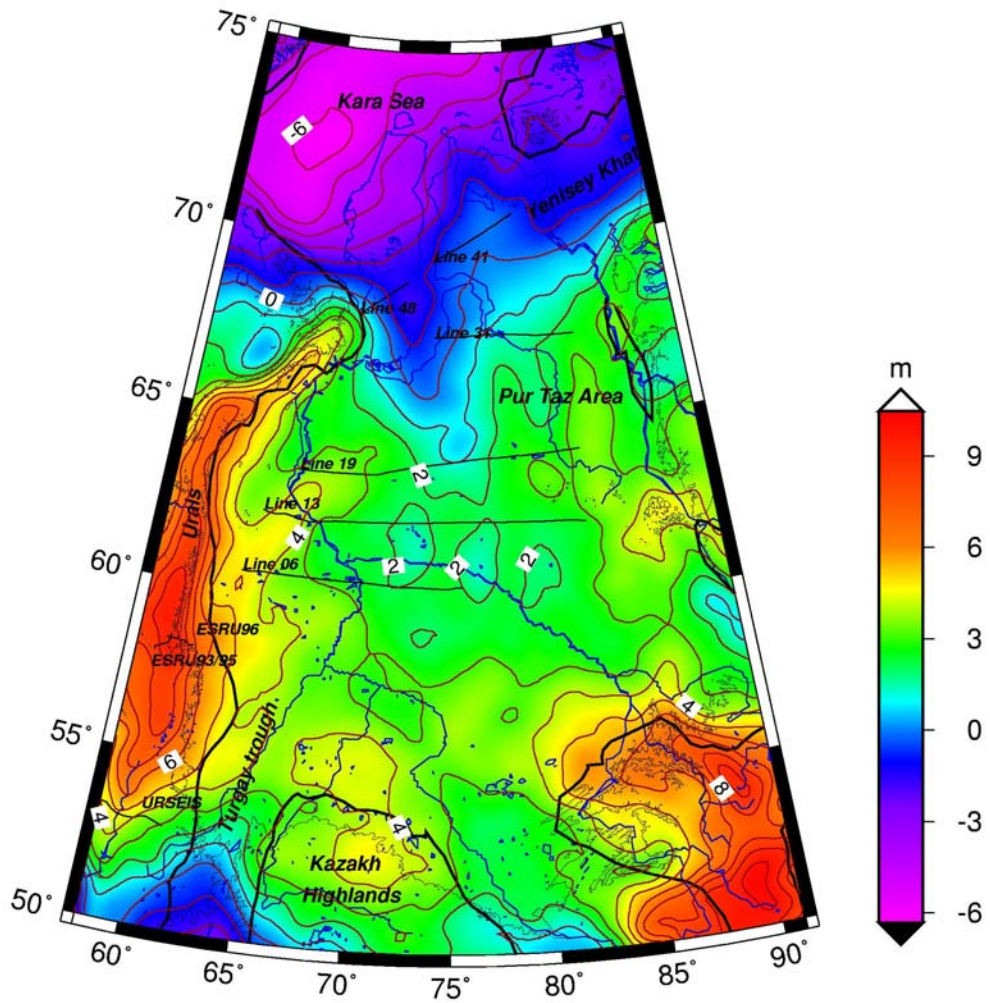


**Figure 5.3** Geoid residual (m) for the West Siberian Basin area. Data: EIGEN-GL04C (Förste et al. 2006) freed from lowest degree and order (up to degree and order 10) harmonic components.



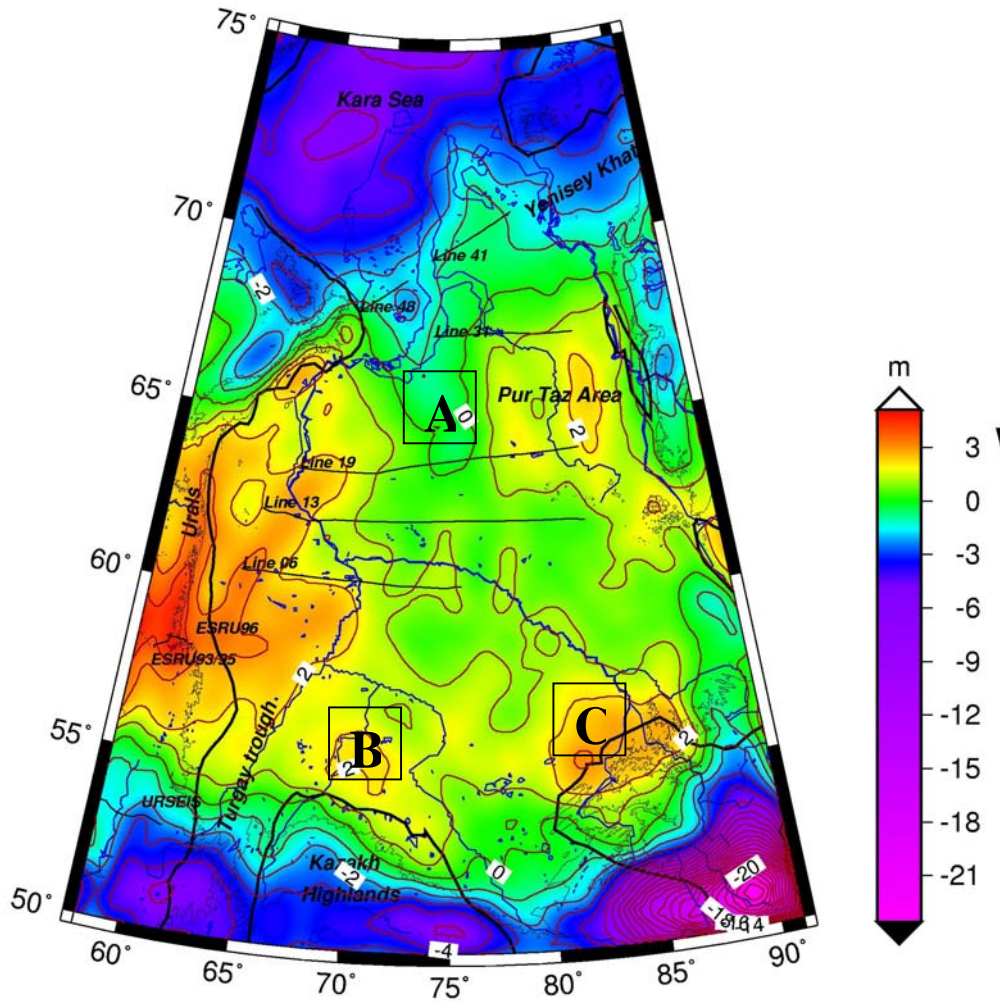


**Figure 5.4** Geoid residual terrain corrected (m) for the West Siberian Basin area. Data: EIGEN-GL04C (Förste et al. 2006) freed from lowest degree and order (up to degree and order 10) harmonic components. A: geoid low correlates with the deepest part of the basin. B, C: geoid highs correlate with shallow basement.

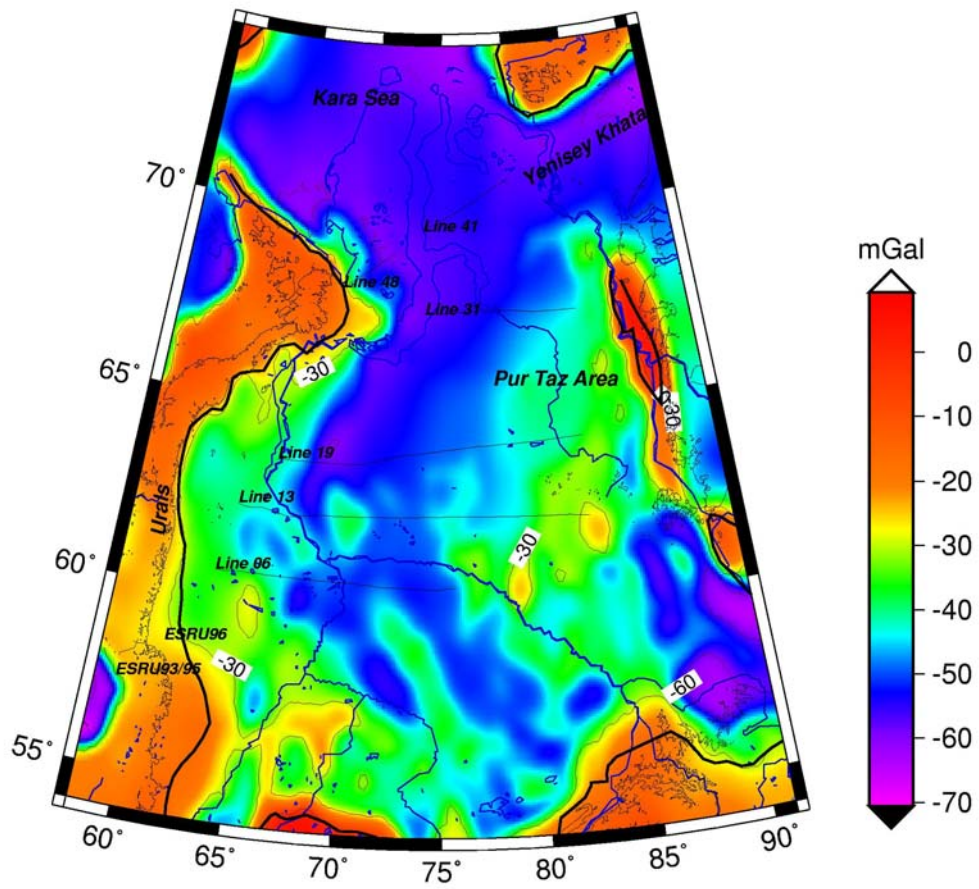


*Figure 5.5 Gravity effect of sediment-package. Linear density increase with depth.*

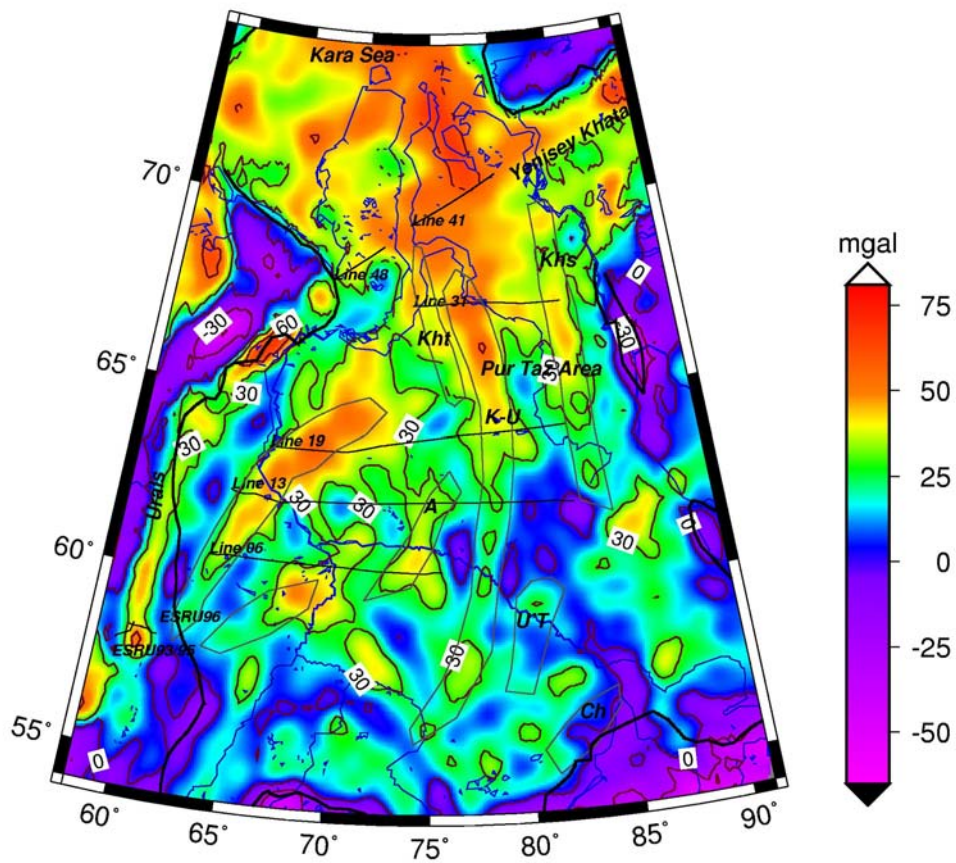


**Figure 5.6** Gravity residual: Bouguer anomaly reduced for the sediment package. Linear density increase with depth of sediments. Seismic lines and supposed graben-rift structures as in Fig. 5.1.

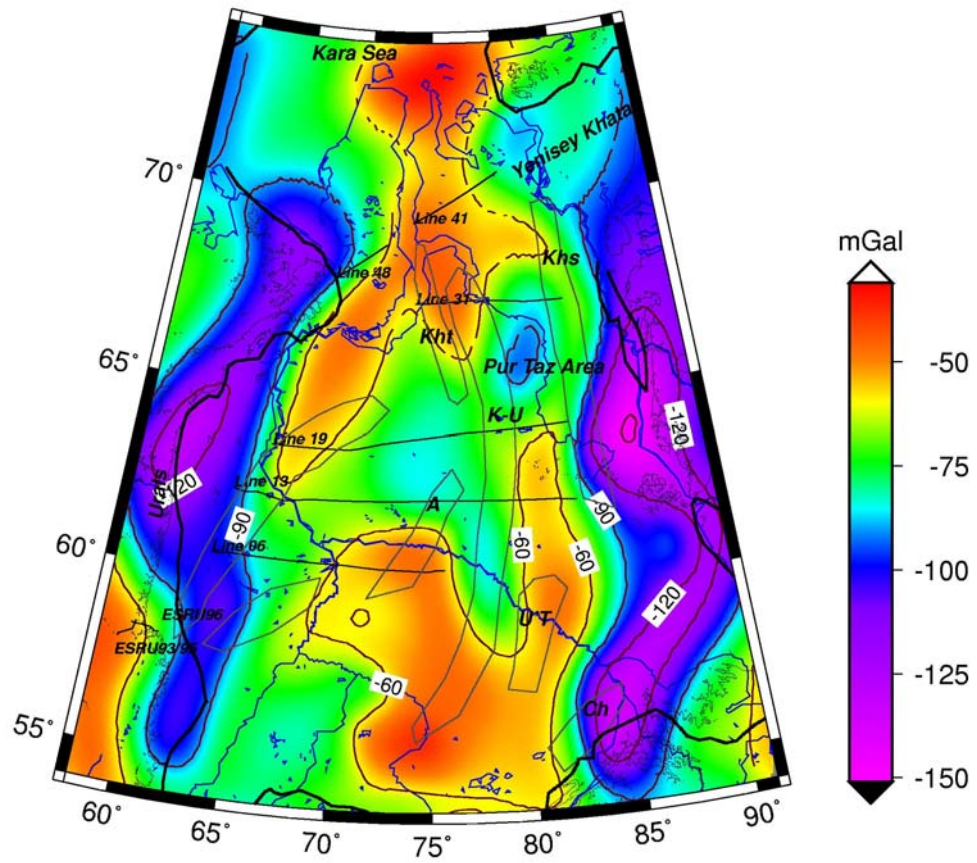


*Figure 5.7 Gravity effect caused by density contrast at the Moho interface. Reference depth =35 km, density contrast:  $0.35 \text{ kg/m}^3$ . Seismic lines and supposed graben-rift structures as in Fig. 5.1.*

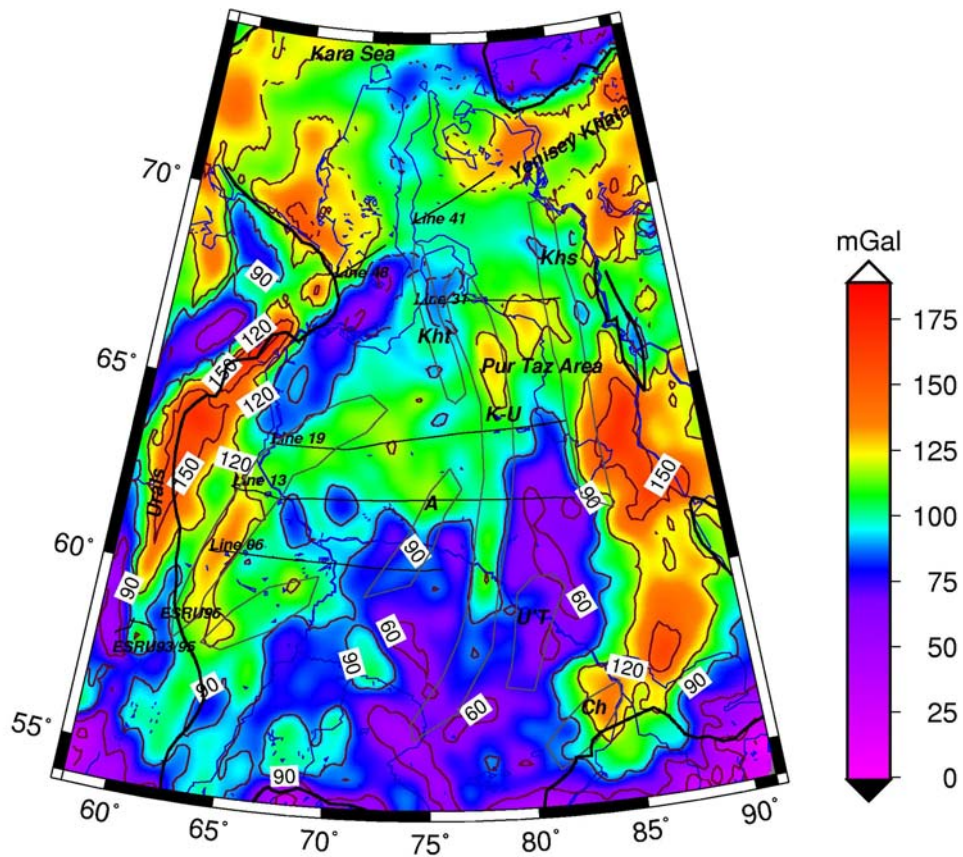


**Figure 5.8** Gravity residual: corrected for topography, sedimentary rocks and crustal thickness variations. Moho reference depth=35 km, Moho density:  $350 \text{ kg/m}^3$ . Also shown are regional seismic profiles and the proposed graben-rift structures (grey; after Pavlov, 1995). Names of rifts: K-U, Koltogory-Urengoi; Khs, Khudosei; Kht, Khudottei; A, Agan; U'T, Ust' Tym; Ch, Chuzik.

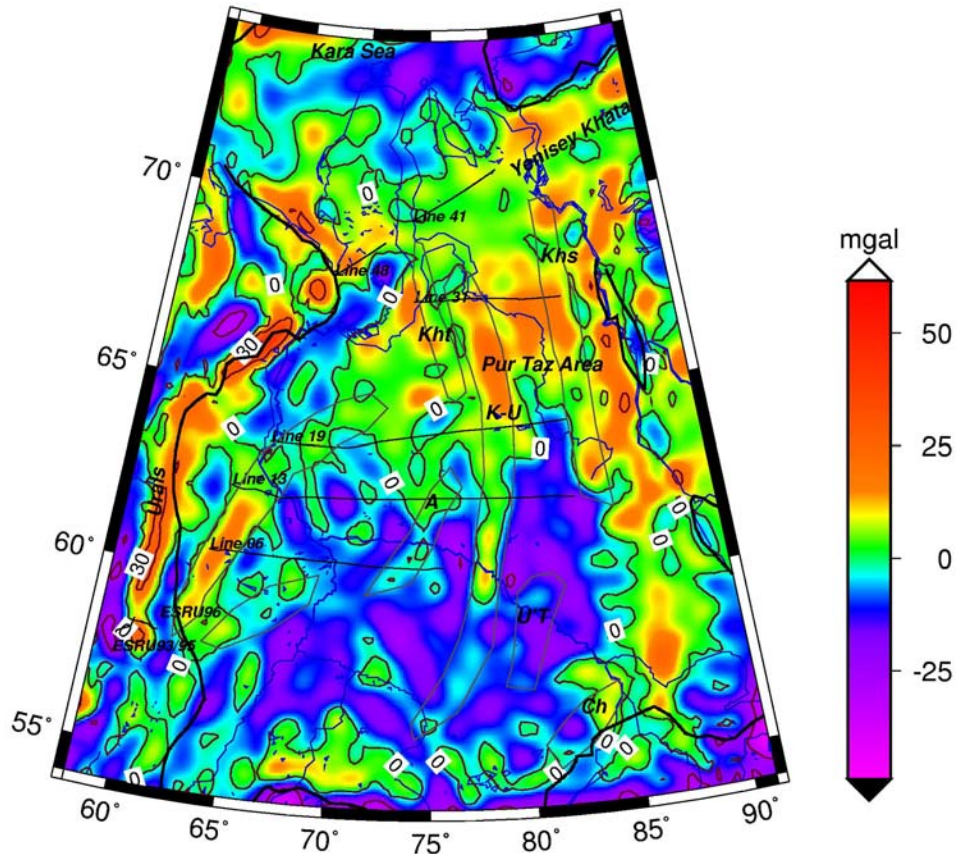


**Figure 5.9** High pass filtered gravity residual, including the correction of the Bouguer anomaly for sedimentary rocks and crustal thickness variations. Also shown are regional seismic profiles and the proposed graben/rift structures (grey; after Pavlov, 1995). Names of rifts: K-U, Koltogory-Urengoi; Khs, Khudosei; Kht, Khudottei; A, Agan; U'T, Ust' Tym; Ch, Chuzik.

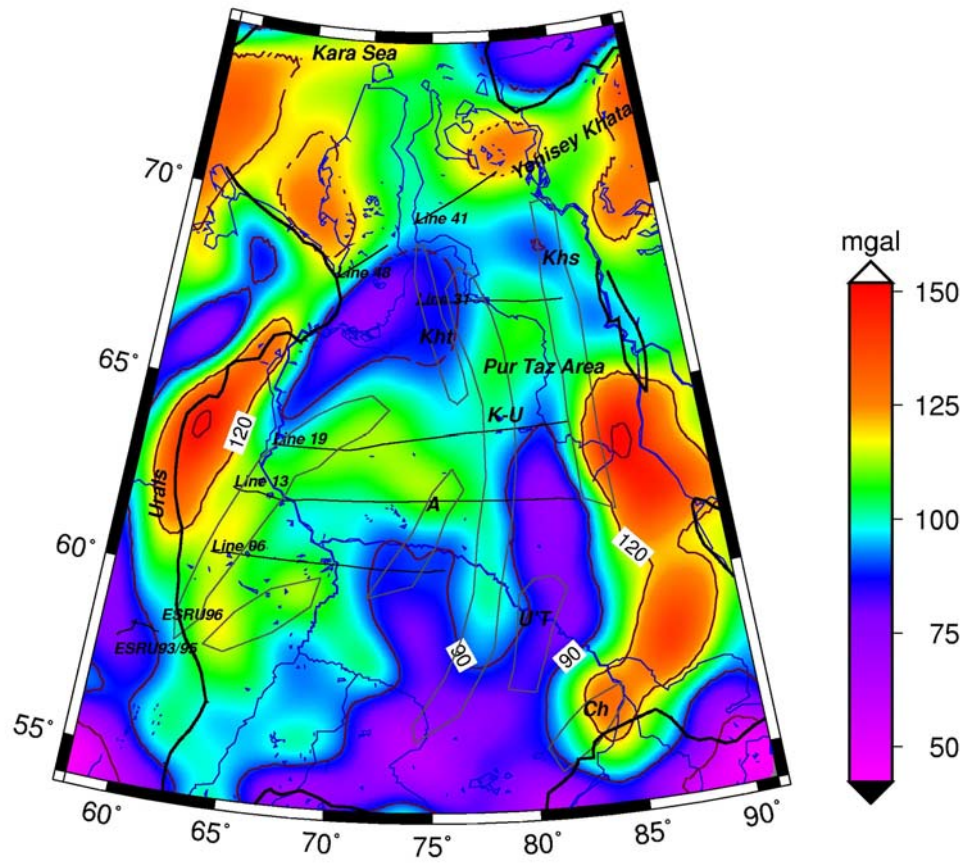


*Figure 5.10* Low pass filtered gravity residual, including the correction of the Bouguer anomaly for sedimentary rocks and crustal thickness variations. Seismic lines and supposed rift structures as in Fig. 5.1.

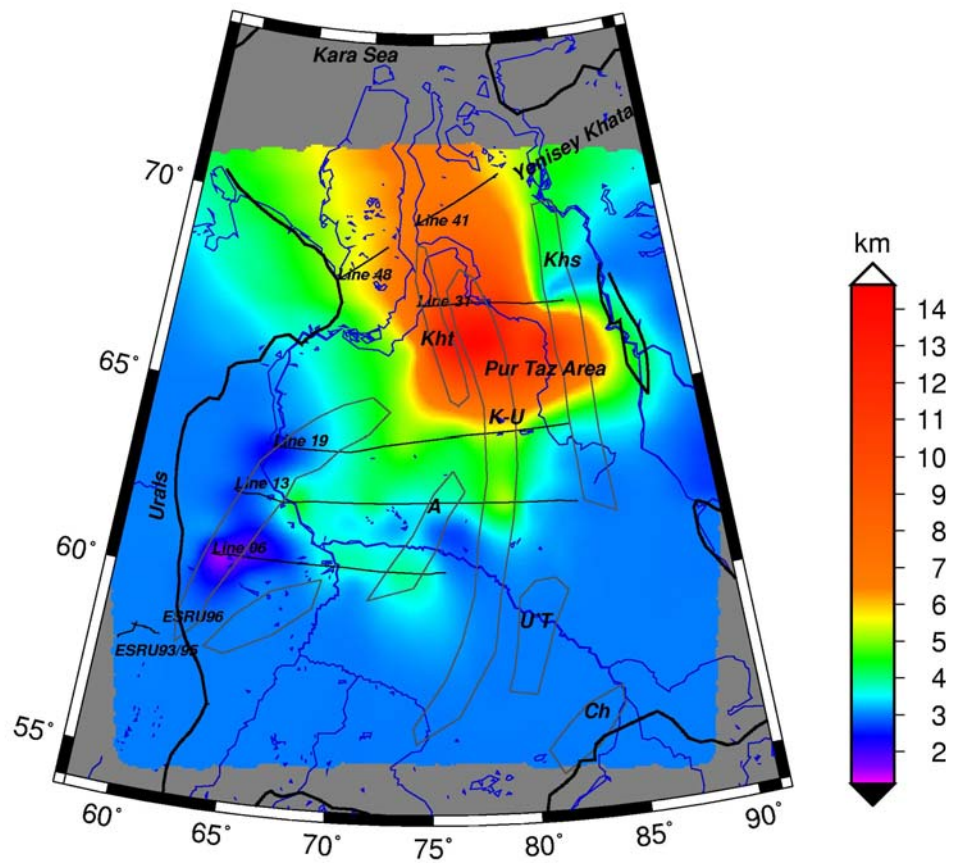


**Figure 5.11** Tentative map of the depth to the base of the basalt layer – the depth is only constrained along the profiles shown in the figure. Seismic lines and supposed graben-rift structures as in Fig. 5.1.



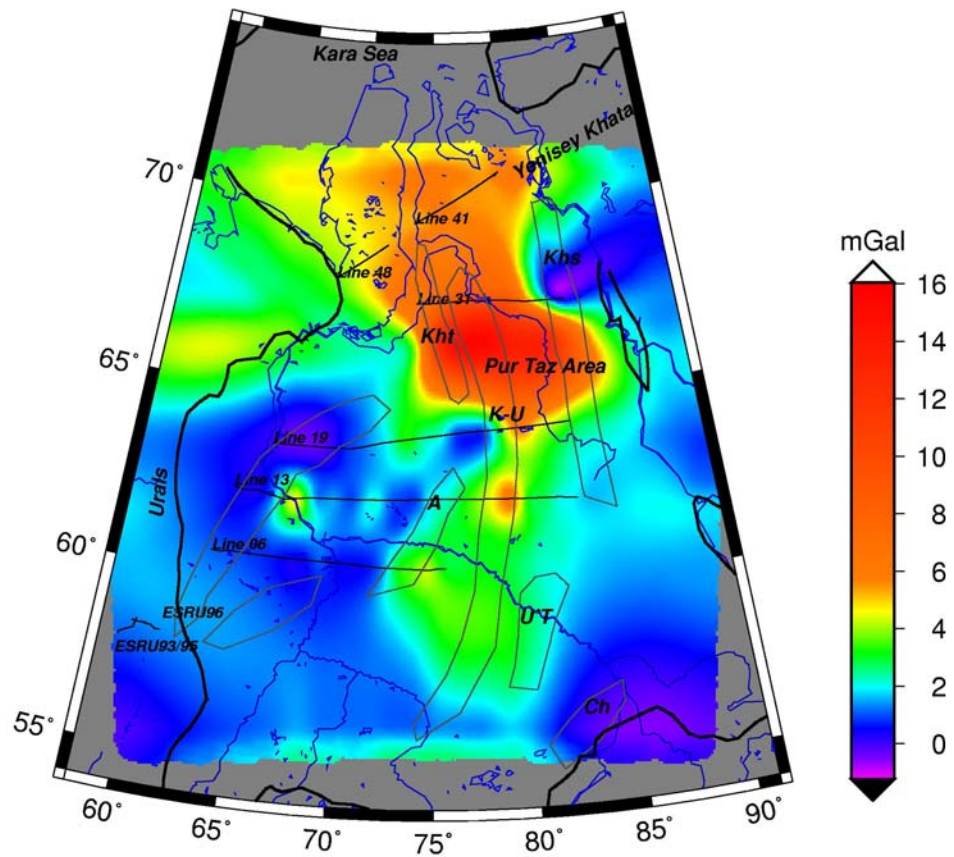


*Figure 5.12* Tentative estimate of the order of magnitude of the gravity signal produced by the basalt layer. Seismic lines and supposed graben-rift structures as in Fig. 5.1.

## 6 GRAVITY INVERSION

In the previous chapters we have shown that the observed gravity field cannot be explained by the sediments and by the crustal thickness variations alone. We come to this conclusion because the residual field is very different from zero and has mostly positive values. This implies that there must be a mass surplus in the crust and/or mantle, which we have not yet accounted for assuming that the applied field reductions are correct. Apart from the problem of assigning the origin of the missing mass, we are now able to distinguish geological provinces of the West Siberian Basin that have different characteristics in crust and basement, without revealing these differences in a topographic expression. In fact the West Siberian Basin has very subdued topography (altitude range less than 200 m), although the variations in the residual gravity field are substantial (roughly 150 mGal range variations).

### 6.1 Lower crustal density variations

We make an approach to explain the residual gravity field by a density increase in the lower crust. For this purpose we invert the residual gravity field to a layer with variable density located just above the Moho, and having 20 km thickness (Fig. 6.1). To adjust the gravity field an overall density increase in the range between  $80 \text{ kg/m}^3$  and  $200 \text{ kg/m}^3$  is needed. The overall density increase from the inversion is related to the fact that the crustal thickness is greater than 35 km, the reference crustal thickness. The crustal thickening implies the presence of crustal material, less dense than the mantle, at mantle depths, thus producing a negative gravity anomaly. Choosing a deeper reference depth would allow to make the density increase start from zero value instead of from the value of  $80 \text{ kg/m}^3$ , thus having the effect of a downward shift of the resulting density anomalies. The density excess needed to explain the observations amounts to  $200 \text{ kg/m}^3$ .

The most prominent density increase is found below the Urals and along the southeastern margin of the basin, flanking the transition to the Siberian craton. The Pur Taz region is also characterized by a moderate density increase, which protrudes southwards and southwestwards. The southwestern density increase is found over a broad area. The area to the east of the Urals emerges with increased density, which coincides in position with the western ends of Profiles 19, 13 and 06. Another area with increased density is found along the Yenisey Khatanga trough. It is very likely that the gravity high of the Pur Taz area can be explained by the thick basalt layer, which in this area presumably has a thickness of about 2

km. As shown above, the 2 km basalt layer accounts to up to 16 mGal, which is in the order of the observed residual anomaly. Along Profile 19 this is probably not the case, so here other high density masses must be invoked, as the basalt layer probably is too thin to produce the observed anomaly.

## **6.2 Upper crustal density variations**

In the previous chapter we have observed that the gravity residual, i.e. the gravity field reduced from the gravity signal of the sediments and crustal thickness variations, presents several linear features. They are very likely to be correlating with the inferred graben-structures (e.g. Allen et al. 2006). We have seen from the seismic profiles and the sections across the sediment thickness grid, that the inferred graben structure in some cases is well distinguishable in the morphology of the basement, inducing a locally thickened basement. The Perm-Triassic boundary is only moderately affected by the graben structures, implying that the graben structures are older than the basalt layer. Saunders et al. (2005), referring to Kontorovich et al. (1975) report that the precise timing of the rifting is unknown, but is thought to be late Permian to early Triassic, approximately coeval with the basaltic volcanism. They further assume that rifting at least continued into the Triassic. An interesting question is, to what extent the graben structures are filled with volcanic and sedimentary rocks, respectively. The volcanic rocks should contribute to a positive, the sedimentary rocks to a negative gravity signal. We tentatively interpret the residual anomalies with positive or negative masses located below and above the reference level. By this approach we can apply a gravity inversion, which leads to the result shown in Fig. 7.2. The inversion was made using the high-pass filtered residual Bouguer gravity field (corrected for sediments and crustal thickness), a reference level of 5 km, and a density contrast to the surrounding of  $300 \text{ kg/m}^3$ . The masses have varying depth extent. In this case, the positive masses can be interpreted as a magmatic body, whereas the negative masses can be anyrocks that have a density less than the crustal reference density.

We come to the conclusion that the depth extension of the basalt layer must be up to 3 km. The greatest thickness is found in the Pur Taz area and in the inferred graben-rift structures, already discussed in the previous paragraphs (e.g. Fig. 5.1). The Pur Taz area is pronounced by three NS to NW-SE trending linear structures, in which the basalt layer thickens. One of these coincides with the Koltogor Urengoy structure, and continues southwards, where after an initial shallowing to almost zero, it resumes thickness of up to 1.9 km in its southernmost

part. Another interesting feature is the linear basalt thickening of up to 2.5 km thickness in the proposed rift structure to the west of the Agan rift. This rift structure has also been proposed by Allen et al. (2006), from the interpretation of magnetic data, whereas it is not mentioned by Pavlov (1995), due to the fact that it is located to the west of his study area. We find a discordance with respect to the Pavlov (1995) when considering the Khudottey rift: According to our inversion, we find a basalt thickening of up to 2.5 km located westwards with respect to the Khudottey rift proposed by Pavlov (1995), whereas in correspondence to this latter feature no thickening is found. Also observing the other fields as a gravity anomaly, or residual Bouguer anomaly, this feature is not evident. We thus propose that the Khudottey rift as mentioned by Pavlov (1995), in reality is shifted to the west by near to 100 km.

### **6.3 Structural elements inferred from the inversion**

The comparison of the lower crustal densities with the basalt-thickness allows distinguishing terranes that presumably involve the entire crust. The rift-graben structures are partly filled with basalt, and are underlain by high density crustal rocks: the Pur Taz area, the Koltogor Urengoy graben, are underlain by crustal rocks with moderately high density (+170 kg/m<sup>3</sup>). The Yenisey-Khatanga trough is underlain by strongly increased lower crustal density (+200 kg/m<sup>3</sup> density increase). The inferred graben to the west of the Pur Taz area, which we have identified with the Khudottey graben is different, as it is located in a broad area in which the density of lower crust has only a slight increment (140 kg/m<sup>3</sup> density increase). The proposed rift structure to the east of the Urals again has increased lower crustal density (190 kg/m<sup>3</sup> density increase). Enigmatic is the well developed structure along the eastern border of the basin towards the Siberian craton, where the elongated superficial high density structure extends for more than 1500 km and is underlain by an arch-formed lower crustal body of extremely high density (220 kg/m<sup>3</sup> density increase). The superficial linear high density structure could be interpreted as basalt, as in its southern sector basalt has been verified by boreholes (Vyssotski et al. 2006).

The final calculated gravity field (Fig. 6.3), that represents the contributions of the crustal model including sedimentary rocks, crustal thickness variations, upper crustal masses (wavelengths between 50 and 150 km), and lower crustal density variations (wavelengths greater than 150 km) differs from the Bouguer field in the order of 30 mGal.

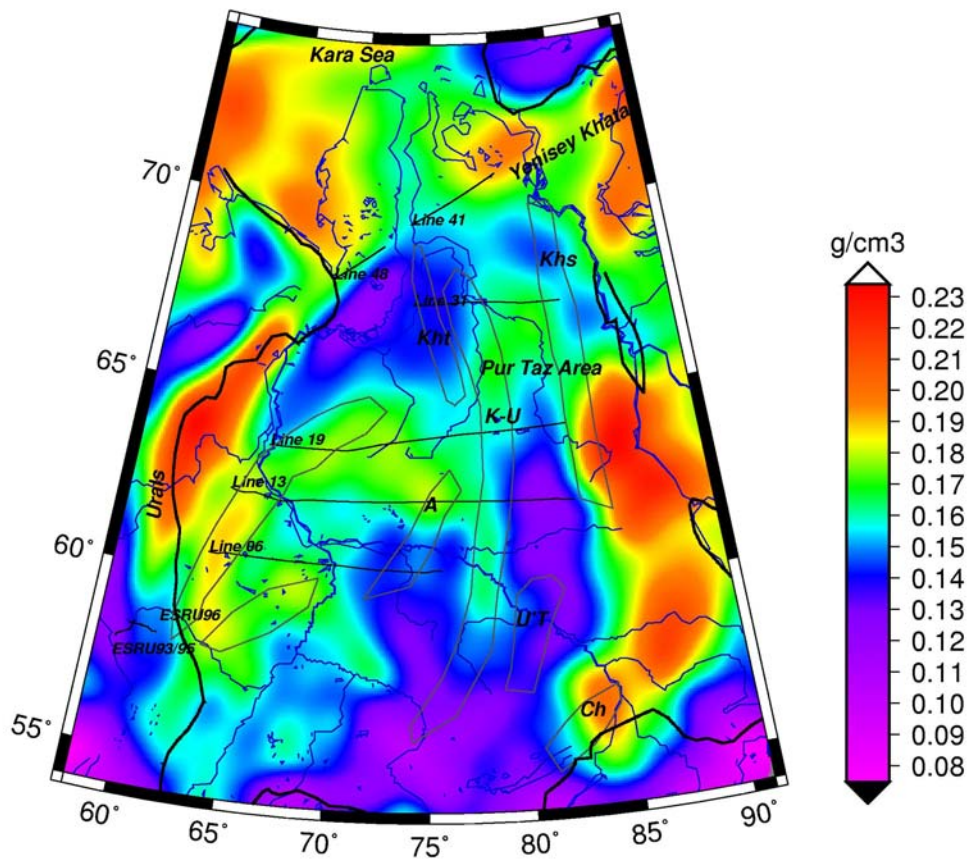


**Figure 6.1** Lower crustal density variations calculated by inverting the residual gravity signal (Fig. 5.8). The density variations are assumed to be in a lower crustal layer extending from the Moho to 20 km upwards. Seismic profiles and supposed -rift structures as in Fig. 5.1.

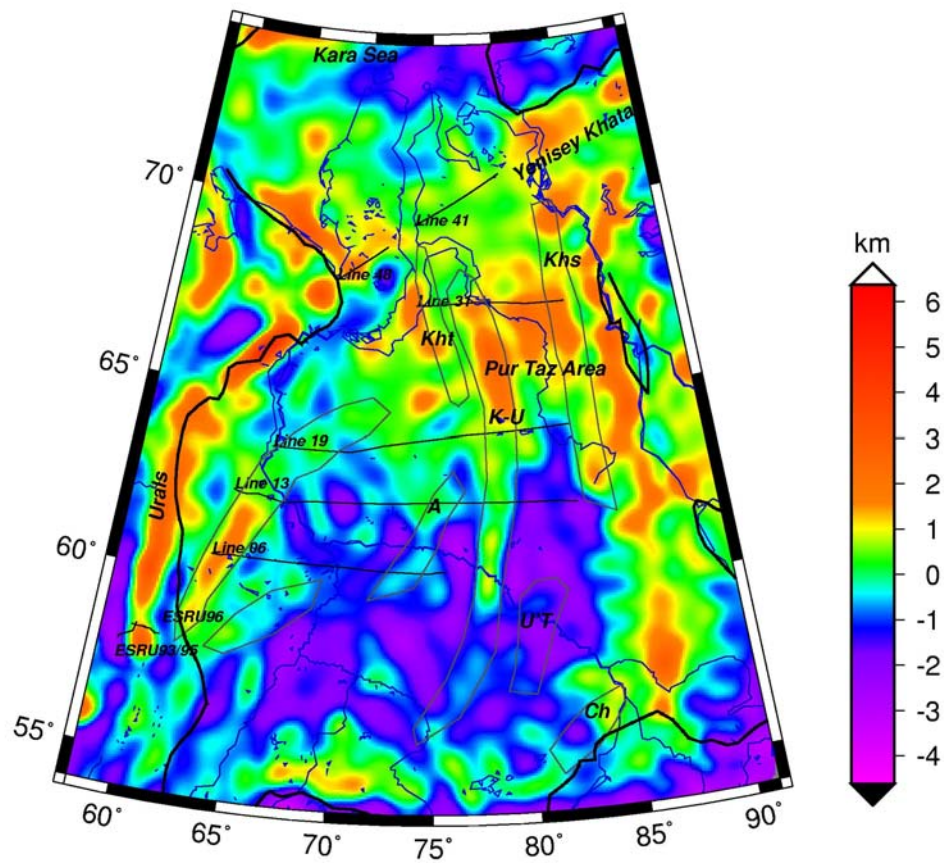


**Figure. 6.2** Upper crustal possible basalt layer obtained by inverting the high-pass filtered residual gravity signal (Fig. 5.9). The masses are assumed to have a density contrast of  $300 \text{ kg/m}^3$  to the surrounding basement and being located at a reference depth of 5 km. Negative thicknesses are equivalent to a layer of equal thickness but with a negative density contrast.

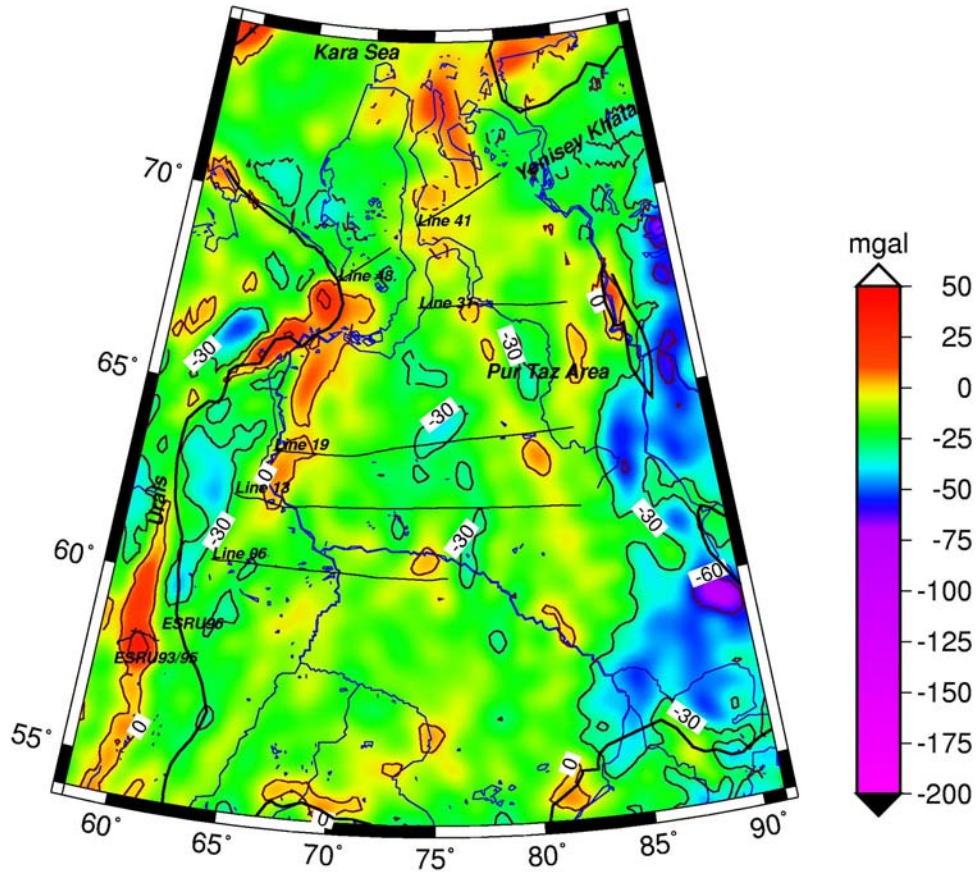


**Figure 6.3** The gravity field produced by the crustal model including sedimentary rocks, crustal thickness variations, upper crustal masses (wavelengths between 50 and 150 km), and lower crustal density variations (wavelengths greater than 150 km). Compare to the Bouguer anomaly (Fig. 5.2).

## 7 ISOSTATIC STATE

### 7.1 Isostatic crustal thickness

We have seen, that the sediment thickness model and the given Moho depth do not explain the Bouguer field, as a strong positive residual remains. We consider now, to what extent the given crustal thickness variations comply with an Airy isostatic model. The topographic load and the sediment model are summed to calculate the total load. We assume the topographic load density and mantle density equal to  $2700 \text{ kg/m}^3$  and  $3300 \text{ kg/m}^3$ , respectively, and a reference depth of 35 km. In Fig.7.1 the isostatic Moho is shown, that is much shallower than the published Moho by Vyssotsky et al. (2006; Fig. 3.4), especially in the northern part of the basin. Furthermore we find that the Airy isostatic Moho over the basin is rather flat, with variations between 32 km and 34 km. Deeper values for the Moho are found along the Urals and along the eastern basin border to the Siberian Platform. In comparison, the published Moho (Fig. 3.4) shows much greater amplitude variation below the basin (34 km to 45 km) and is more articulate, dividing the basin into different areas, irrespective of the fact that the basin topography is flat. The evident mismatch of the Airy isostatic Moho and the observed Moho can be interpreted in two ways: either the isostatic model does not apply for the West Siberian Basin for a reason still to be understood, or the observed Moho is already an isostatic response to the buried masses within the crust.

### 7.2 Isostatic gravity anomaly

By subtracting the gravity field of the isostatic Moho from the Bouguer anomaly, we obtain the isostatic anomaly, which is a more common expression of the isostatic state of an area (Fig. 7.2). The density contrast between crust and mantle is assumed to be  $350 \text{ kg/m}^3$ . The Airy isostatic anomaly has the following features: its values are all positive, ranging between 0 and 175 mGal. The anomalies are largely independent from the topography, which implies that the flat basin conceals buried masses. The greatest positive anomalies of the basin are found along its eastern border with the Siberian Platform. The western border of the basin, along the Urals, is a second strongly positive anomaly. This latter anomaly partly has a topographic counterpart. The Pur Taz area shows moderately positive anomalies, from which the Koltogor-Uengoy graben extends southwards. A broad SW-NE trending positive anomaly extends from the Pur Taz area across the basin. The transition to the Kara Sea is smooth and does not reveal tectonic borders.



The fact that the isostatic anomaly is so different from zero shows that the load model consisting of topography, sediments and a crustal thickness variation according to the local Airy model of compensation does not apply here. Our interpretation of this observation is, that there are buried masses that contribute to the isostatic equilibrium and that have an expression in the observed gravity field, similar to our analysis in Ch. 6.

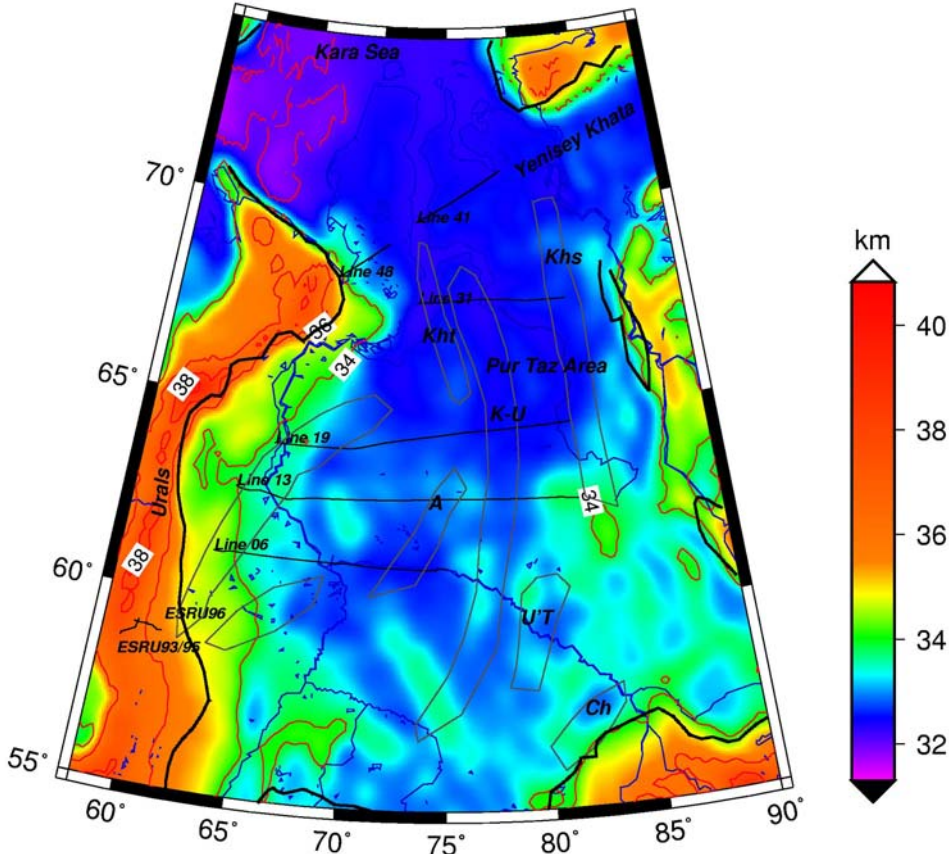


*Figure 7.1 Isostatic Moho, considering the sedimentary and the topographic load. Reference depth = 35 km.*

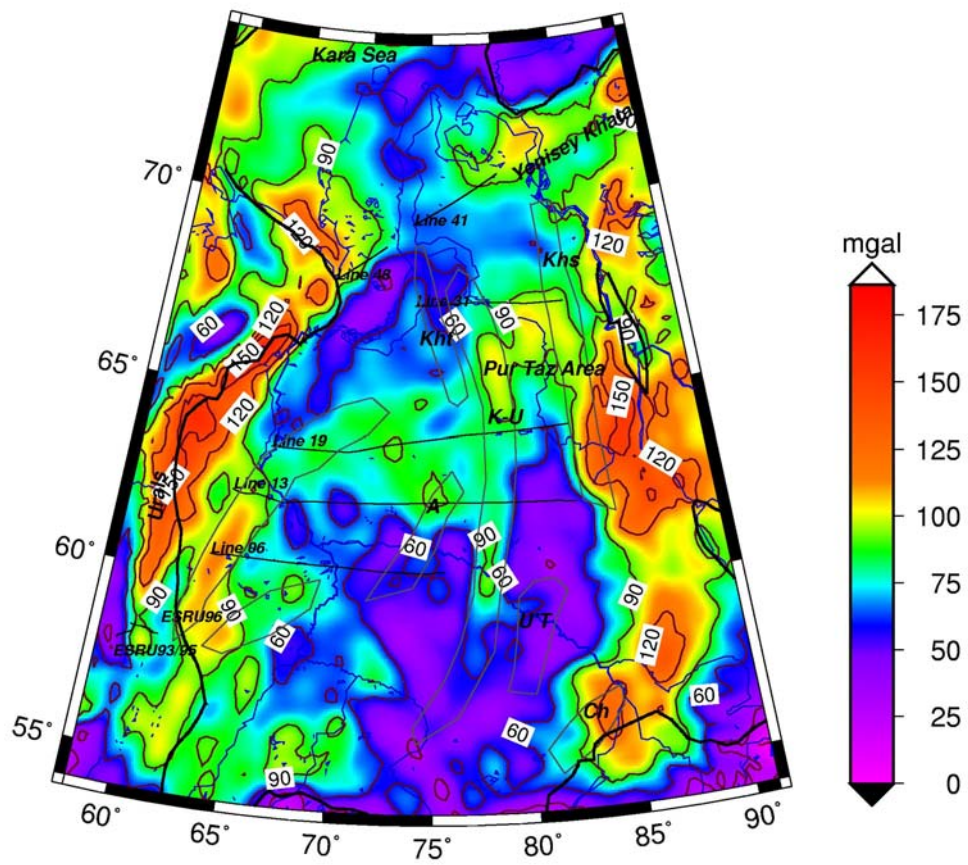


*Figure 7.2. Isostatic gravity anomaly.*

## 8 CONCLUSION AND OUTLOOK

The present study aims at identifying the crustal units that constitute the West Siberian Basin. A review of the existing literature shows that the basement-units underlying the sediments are poorly known. The basement is thought to consist of an assemblage of rock types ranging in age from Proterozoic to Upper Paleozoic. The terrane blocks comprise fragments of island arcs, microcontinents and relict ocean basins (Saunders et al. 2005; Peterson and Clarke, 1991; Sengor and Natal'in, 1996). Even the sedimentary deposits are known only partially, due to their great depth extent (more than 15 km), which makes the detection of the basement difficult. Moreover the presence of the late Perm - early Triassic basalt layer, acts as a screen to the investigation of the older sedimentary layers. The basalt layers are only partially known and the uncertainty on their areal extent is 100%, that of the thickness being even greater. Evidence for the presence of basalt is given by boreholes in sparse regions of the basins, which penetrated the basalt. It is presently unknown, where the focus of the basalt is (if a focus exists), the Pur Taz area having been proposed to have been one (Saunders et al. 2005). From evidences in seismic lines and in the gravity and magnetic fields, several rift-graben structures have been proposed, that have a NS or NE-SW orientation. Among different authors there are some discrepancies in the exact location of the rift structures (e.g. Surkov et al. 1982; Pavlov, 1995; Surkov, 2002; Nikishin et al. 2002; Allen et al. 2006; Vyssotski et al. 2006). The older papers limit these structures to the central part of the basin, with no extension westward towards the Urals. The amount of sediments and volcanic material filling the graben/rifts is still uncertain. Another question is the role of the rift-graben structures in the production of the basalt: whether the basalt has formed in these structures, whether it propagated outwards in the subsurface as dykes or whether it flowed at the surface (Saunders et al. 2005). Unknown is also whether the rift structures have a characteristic crustal feature underlying them, which is affecting the crustal thickness and the physical properties as density, rheology, heat production, and physical conditions. Clearly there exist still a large number of unknowns in our understanding of the different blocks of the West Siberian Basin, and consequently its formation history. However, the results of our study contribute to the knowledge of the crustal structure, as we are able to differentiate the basin into several units, which are well distinguished in terms of superficial and deep density structure. Our analysis allows to image to a certain degree the extent of basalt and to image the buried rift topology below the West Siberian Basin.

We have used the gravity anomaly, the geoid and the isostatic conditions to characterise the crustal structure. We used the recently greatly improved gravity field solution derived from the integration of the satellite GRACE with terrestrial data (Förste et al. 2006; Tapley et al. 2005). When dealing with satellite data all calculations ought to be made above the existing topography.

Essential for the study is the correction of the gravity field for the sedimentary layers and the crustal thickness variation. Here an important distinction is, whether the sedimentary layers preceding or succeeding the basalt layer are considered. We have obtained gridded data for the pre-basalt layers and relied on the publication of Vyssotski et al. (2006) for the post-basalt layers, digitising the published seismic lines. The comparison of the bottom of these two units is very interesting, as it reveals that the deepening of the lower sediments associated with the rifting, is not evident in the post-volcanic layers. This is evidence to the fact that the accumulation of the post-volcanic layers were tied to a large scale subsidence, after the rifting ceased (e.g. Artyushkov and Baer, 1986).

Another data set that we included in our study was the crustal thickness. With these data at hand, we have proceeded to reduce the gravity and geoid fields for the effect of topography, sedimentary rocks and crustal thickness variations. The calculations for topography and crustal thickness are straightforward, and were made assuming a laterally constant density.

The correction for the gravity effect of the sedimentary rocks required some effort, as the density increase with depth has to be considered. For this purpose we have used the well information on horizon depths, to invert for the depth variation of velocity. Empirical velocity-density relations were then used to estimate the density-depth variation.

At this point we have compared the gravity field of the crustal model, which includes all known masses with the observed field. We find large residual anomalies, up to roughly 150 mGal, demonstrating the presence of masses with increased density located in the crust. It is improbable that the position of the density anomalies will be in the mantle, as the seismic investigations (Morozova et al. 1999) give some indication that the mantle below the West Siberian crust has a low velocity anomaly. The distribution of wavelengths of the residual field is such, that we propose these masses to be located both in lower and upper crust. The

basalts, which are high density bodies, cannot explain all of the residual signal, as we estimate that they contribute to not more than 16 mGal.

When we consider the larger wavelengths (greater or equal 150 km), and interpret these as stemming from density variations in the lower crust, we obtain a segmentation of the basin, which we summarise in Fig. 8.1. We find an arch-shaped density increase along most of the eastern border of the basin (Arch, Fig. 8.1) and along the western border, along the Urals. The eastern structure could fit the Baykalides, a unit mentioned in the generalized tectonic map by Sengor and Natal'in (1996) displayed in Vyssotski et al. (2006). The lower crustal density variation in the basin leads to identify the southern and mid-western segment (slightly increased density), the middle segment, including the Pur Taz area (moderately high density), and the northern segment (moderately high density).

We draw conclusions also from the short-wavelength residual gravity field (wavelength less than 150 km). We invert the residual field in terms of a mass located a few km below the surface (5 km reference depth). On the basis of the existing literature, we may confidently interpret linearly extending positive masses as rift units. The above mentioned rifts, the most evident being the Koltogor-Urengoy, the Khudotey, and the Khudosey emerge well in the inversion. The inversion reveals a few other well developed structures: a very prominent structure extends for more than 1500 km length along the eastern border of the basin. It partly runs along the Yenisey river, so we may call it the Yenisey graben. It overlaps and crosses the eastern arch mentioned above. The Yenisey graben is located east of the Khudosey rift, an observation made already by Allen et al. (2006) from the interpretation of magnetic data. At its northern end the Khudosey rift bends eastward into the Yenisey-Khatanga trough. Across the trough we find a symmetrically located graben (Fig. 8.1). Of interest is also the NE-SW trending rift-graben structure we find in the western part of the mid-basin. It produces a prominent gravity signal and lies in the area of increased lower crustal density. Fig. 8.2 shows the magnetic field anomaly of the West Siberian Basin.

The rift structures we find seem to be only partly correlated with the lower crustal density variations-. In fact they cross the basin segments as defined above. This could be an indication that the rift-graben structure is overprinting older crustal blocks, the latter being differentiated in their lower crustal densities. A few units do correlate, as the Yenisey rift

that overlies the Arch, and the mid-basin segment that trends SW-NE, and which carries rift structures of the same orientation.

Concluding, we are confident of the fact that the availability of the gravity field over the entire basin allowed to improve the knowledge of the structure. The density modelling we have made relies on the input fields, e.g. the Moho variations and the sediment thickness. Presently the Moho and the post-volcanic sediment thickness have been retrieved from the publication of Vyssotski et al. (2006). Due to the strong economic interest in the basin, several more seismic lines exist, to which we presently do not have access. A deepening of the work should include these in the analysis. The present study was focussed on the West Siberian Basin, which we have seen propagates smoothly into the Kara Sea northwards, into the Yenisey-Khatanga trough eastwards, and into the Turgay trough southwards. To complete the study, these extensions should be included in the analysis.

Another aspect to be considered in the future is the joint modelling of the gravity and magnetic fields (Fig. 8.2), which is expected to give a better definition of the rift-graben structures and to give an improved picture of the basement.

The focussed study of the West Siberian Basin was made in the context of a major project that addresses the understanding of cratonic and intracratonic basins (Braitenberg and Ebbing, 2006), and in particular their relation to the Eastern Barents Sea (Ebbing et al. 2005; Ebbing et al. 2006; Ebbing et al. in press). We conclude that in many aspects the West Siberian Basin is very different from the Eastern Barents Sea: the Eastern Barents Sea has smooth near to elliptical sediment isopachs, rift structures are almost absent, and the residual gravity anomalies are much less pronounced. We relate this to a very different composition of the underlying basement and to the fact that rifting in the Eastern Barents Sea was not effective. The extensive flood basalt of the Western Siberian Basin is surely another important aspect, which probably is not present in the Eastern Barents Sea.

One feature is in common, and that is the overall positive residual gravity anomaly, once the Bouguer field has been reduced for the sediments and the crustal thickness variations. This is an interesting point which needs some further investigation. Seismological investigation show that the upper mantle has a high-velocity and density below the West Siberian Basins and

structurally very similar to the observations below the East Barents Sea Basin (Ritzmann et al. 2007). Effort should be made to link these areas in detail and to study both basins in parallel.

For the Eastern Barents Sea the missing mass was ascribed to stem from the upper mantle, whereas for the Western Siberian Basin it was interpreted to be in the lower crust. In both areas, some uncertainties exist, to where to place the needed masses, whether in crust or mantle. In both cases the observed gravity field can be satisfied, so the compatibility with other geophysical or geological information must be investigated. An integrated analysis of both basins could be a viable method to obtain a clearer picture of the tectonic situation.

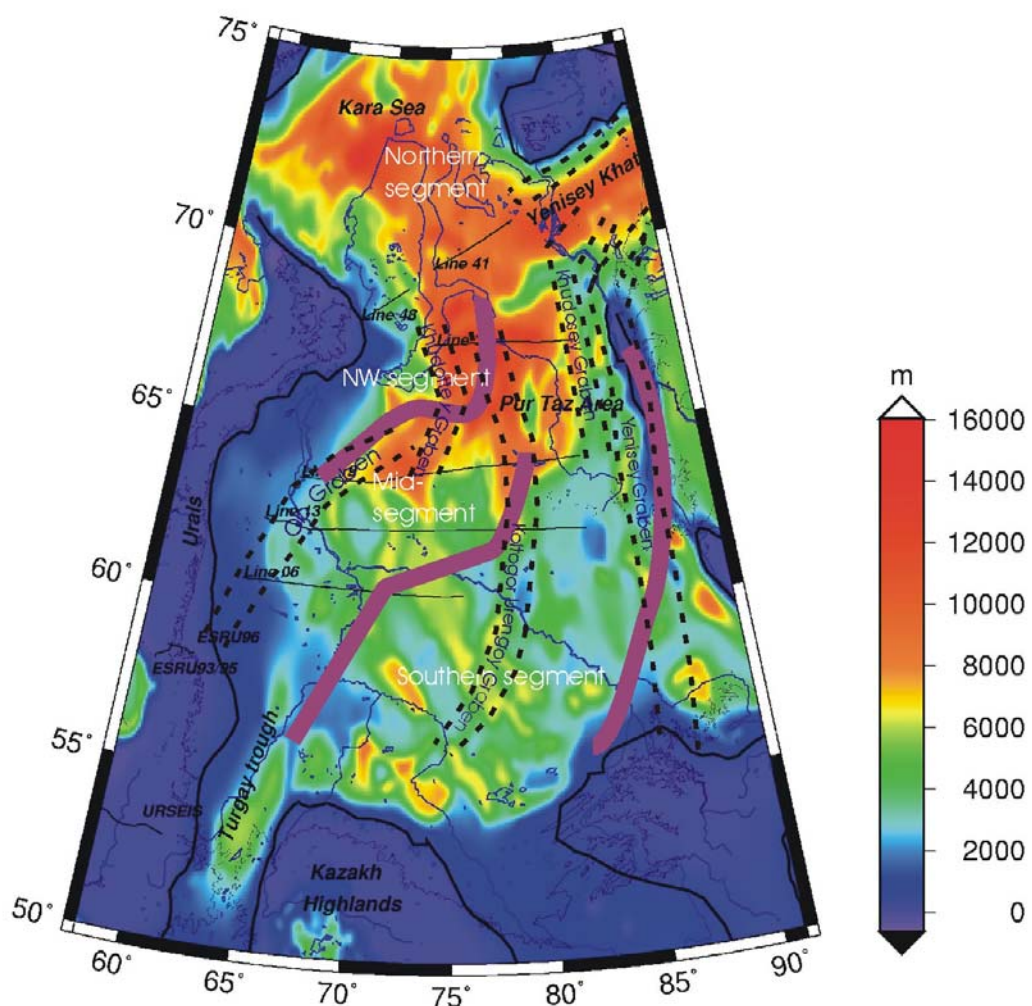


**Figure 8.1** Bottom of pre-volcanic sediments with interpretation of segments composing the basin and principal rift-graben structures.

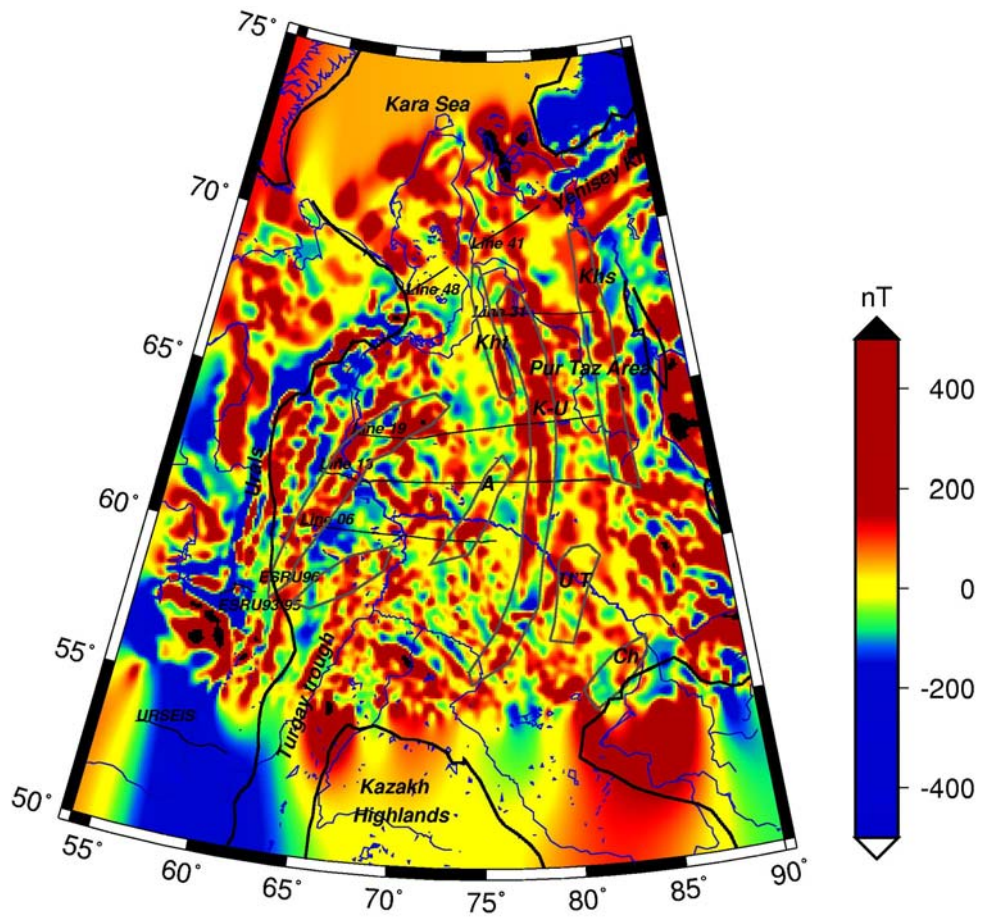


**Figure 8.2** Magnetic anomaly of the West Siberian Basin (data from National Geophysical Data Center, 1997).



## **ACKNOWLEDGEMENTS**

Ildiko' Nagy is thanked for assistance in the bibliographic search and retrieval of documents. Laura Mareello is thanked for making her study on density-velocity relations available. Hans Morten Bjørnseth and Christine Fichler from Statoil initiated our study and supplied us with information on the West Siberian Basin. Øyvind Steen from Statoil is thanked for the data on sediments thickness. We appreciate the assistance and help from all these persons and especially Statoil for funding the study. We acknowledge the use of the GMT-mapping software by Wessel and Smith (1998).

## **REFERENCES**

- Aplonov, S.V. 1995: The tectonic evolution of West Siberia—an attempt at a geophysical analysis. *Tectonophysics*, 245, 61–84.
- Allen, M.B., Anderson, L. Searle, R.C. & Buslov, M. 2006: Oblique rift geometry of the West Siberian Basin: tectonic setting for the Siberian flood basalts. *Journal of the Geological Society*, London, 163, 901-904.
- Artyushkov, E.V. and Baer, M.A. 1986: Mechanism of formation of hydrocarbon basins: the West Siberia, Volga-Urals, Timan-Pechora basins and the Permian basin of Texas. *Tectonophysics*, 122, 247-281.
- Bassin, C., Laske, G. & Masters, G. 2000: The Current Limits of Resolution for Surface Wave Tomography in North America. *EOS Trans AGU*, 81, F897.
- Braitenberg, C., Wang, Y., Fang, J., & Hsu, H.T. 2003: Spatial Variations of flexure parameters over the Tibet-Quinghai Plateau. *Earth Planet. Sci. Lett.*, 205, 211-224.
- Braitenberg C., Wienecke S. & Wang Y. 2006: Basement structures from satellite-derived gravity field: South China Sea ridge. *Journal of Geophysical Research*, Vol.111, B05.
- Braitenberg, C & Ebbing, J. 2006: A study of large-scale basins and comparison to the Eastern Barents Sea basins. *NGU Report 2006.081*, p.71.
- Braitenberg, C. & Ebbing, J. 2007: The gravity potential derivatives as a means to classify the Barents sea basin in the context of cratonic basins. *Extended Abstracts, EGM 2007 International Workshop, Innovation in EM, Grav and Mag Methods: a new Perspective for Exploration, Villa Orlandi, Capri - Italy, 15-18 April 2007* (<http://www2.ogs.trieste.it/egm2007/>)
- Braitenberg C., Wienecke S, Ebbing, J., Born, W. & Redfield, T. 2007: Joint gravity and isostatic analysis for basement studies - a novel tool. *Extended Abstracts, EGM*

- 2007 International Workshop, Innovation in EM, Grav and Mag Methods: a new Perspective for Exploration, Villa Orlandi, Capri - Italy , 15-18 April 2007 (<http://www2.ogs.trieste.it/egm2007/>),
- Brink, H.-J. 2005: The evolution of the North German Basin and the metamorphism of the lower crust. *Int. J. Earth Sci. (Geol. Rundsch.)*, 94, 1103–1116.
- Chen, Z.Q. & Shi, G.R. 2003: Late Paleozoic depositional history of the Tarim basin, northwest China: an integration of biostratigraphic and lithostratigraphic constraints. *AAPG Bulletin*, 87, 1323-1354.
- Crust 2.0 2006: <http://mahi.ucsd.edu/Gabi/rem.html>
- Czamanske, G.K., Gurevitch, V., Fedorenko, V., Simonov, O. 1998: Demise of the Siberian plume: palaeogeographic and palaeotectonic reconstruction from the prevolcanic and volcanic record, north-central Siberia. *Int. Geol. Rev.*, 40, 95-115.
- Döring, J. & Götze, H.-J. 1999: The isostatic state of the southern Urals crust. *Geol. Rundsch.*, 87, 500-510.
- Döring, J., Götze, H.-J. & Kaban, M. 1997: Preliminary study of the gravity field of the southern Urals along the URSEIS '95 seismic profile. In: Peres-Estaún, A., Brown, D., Gee, D. (eds.) EUROPROBE's Uralides project. *Tectonophysics*, 276, 49-62.
- Ebbing, J., Braitenberg, C. & Skilbrei, J.R. 2005: Basement characterisation by regional isostatic methods in the Barents Sea. *NGU Report 2005.074*, p.78
- Ebbing, J., Braitenberg, C., Bjørnseth H.M., Fichler, C. & Skilbrei J.R. 2006: Basement Characterisation by Regional Isostatic Methods in the Barents Sea. *EAGE/EAGO/SEG Conference, Saint Petersburg*.
- Ebbing, J., Braitenberg, C., Wienecke, S., in press: Insights into the lithospheric structure and the tectonic setting of the Barents Sea region from isostatic considerations. *Geophysical Journal International*, in press.
- Forsberg, R. 1984: A Study of Terrain Reductions, Density Anomalies and Geophysical Inversion Methods in Gravity Field Modelling. *Reports of the Department of Geodetic Science and Surveying, No. 355, The Ohio State University, Columbus, Ohio, 1984*.
- Förste, C., Flechtner, F., Schmidt, R., König, R., Meyer, U., Stubenvoll, R., Rothacher, M., Barthelmes, F., Neumayer, H., Biancale, R., Bruinsma, S., Lemoine, J.-M. & Loyer, S. 2006: A mean global gravity field model from the combination of satellite mission and altimetry/gravimetry surface data – Eigen-GL04C. *Geophysical Research Abstracts*, Vol. 8, 03462, 2006

- Friberg, M., Juhlin, C., Green, A.G., Horstmeyer, H., Roth, J., Rybalka, A., Bliznetsov, M. 2000: Europrobe seismic reflection profiling across the eastern Middle Urals and West Siberian Basin. *Terra Nova*, 12, 252-257.
- Gramberg, I.S., Glebovsky, V. Y., Grikuro, G.E., Ivanov, V.L., Korago, E.A., Kos'ko, M.K., Maschenkov, S.P., Piskarev, A.L., Pogrebitsky, Y.E., Shipelkevitch; Y. V. and Suprunenko, O.I., 2001: Eurasian Artic Margin: Earth Science Problems and Research Challenges. *Polarforschung* 69, 3-15.
- Gardner, G.H.F., Gardner, L.W., and Gregory, A.R., 1974: Formation velocity and density – the diagnostic basics for stratigraphic traps. *Geophysics*, 39, 770-780.
- Kaban M.K., Schwintzer P., Artemieva I.M. & Mooney W.D. 2003: Density of the continental roots: compositional and thermal contributions. *Earth and Planetary Science Letters*, 209, 53-69.
- Karus, E.V., Gabrielyants, G.A., Kovylin, V.M. & Chernyshev, N.M. 1984: Depth pattern of West Siberia. *Sov. Geol.*, 5, 75-84 (in Russian).
- Kontorovich, A.E., Nesterov, I.I., Salmanov, F.K., Surkov, V.S., Trofimuk, A.A., Erv'ye, Yu.G., 1975: *Geology of Petroleum and Gas in Western Siberia*. Nedra, Moscow. 679 pp.
- Kovylin, V.M. 1985: Fault-block structure of the West Siberian Craton and its petroleum potential. *Sovetskaya geologiya* 2, 77–86. [in Russian].
- Jones, E. J. W. 1999: *Marine Geophysics*. John Wiley and Sons, Ltd., New York, 1-466.
- Larsen, H.C., Saunders, A.D., Clift, P.D. and the Shipboard Scientific Party, 1994: *Proceedings of the Drilling Programme Initial Report*, 152, Ocean Drill. Program. College Station, Texas.
- Lithospheric Dynamic Atlas of China 1989: China Cartographic Publishing House, Beijing.
- Ludwig, W.J., Nafe, J.E. & Drake, C.L. 1970: Seismic refraction. In: *The Sea* (Editor A.E. Maxwell), Vol. 4 (Part 1), Wiley-Interscience, New York, 53-84.
- McKenzie, D. 1978: Some remarks on the development of sedimentary basins. *Earth and Planetary Science Letters*, 40, 25-32.
- Morozova, E.A., Morozov, I.B., Smithson, S.B., Solodilov, L.N., 1999. Heterogeneity of the uppermost mantle beneath Russian Eurasia from the ultra-long-range profile QUARTZ. *Journal of Geophysical Research*, 104 (B9), 20329–20348.
- National Geophysical Data Center 1997: *Magnetic Anomaly Data of the Former USSR*. National Geophysical Data Center, Boulder, CO (CD-ROM).

- Nikishin, A.M., Ziegler, P.A., Abbott, D., Brunet, M.-F. & Cloetingh, S. 2002: Permo–Triassic intraplate magmatism and rifting in Eurasia. Implications for mantle plumes and mantle dynamics. *Tectonophysics*, 351, 3–39.
- Peterson, J.A. and Clarke, J.W. 1991: Geology and hydrocarbon habitat of the West Siberian Basin. *AAPG Studies in Geology # 32*. AAPG, Tulsa, Oklahoma, p. 96.
- Pavlenkova, G.A., Priestley, K. & Cipar, J. 2002: 2D model of the crust and uppermost mantle along rift profile, Siberian craton. *Tectonophysics*, 355, 171-186.
- Pavlov, Yu.A 1995: On recognition of rift structures in the basement of the West Siberian plate. *Geotectonics, English Translation (AGU)*, Vol. 29, no.3, 213-223.
- Reichow, M.K., Saunders, A.D., White, R.V., Al’Mukhamedov, A.I. & Medvedev, A.Y. 2005: Geochemistry and petrogenesis of basalts from the West Siberian Basin: an extension of the Permo–Triassic Siberian Traps, Russia. *Lithos*, 79, 425-452.
- Ritzmann, O., Faleide, J.I., Planke, S. & Myklebust, R., 2007: Geophysical structure of the Barents Sea crust and upper mantle compared to Western Siberia. *Geophysical Research Abstracts*, Vol. 9, 07958, 2007.
- Saunders, A.D., England, R.W., Reichow, M.K. & White R.V. 2005: A mantle plume origin for the Siberian traps: uplift and extension in the West Siberian Basin, Russia, *Lithos*, 79, 407-424.
- Schissel, D. & Smail, R. 2001: Deep mantle plumes and ore deposits. In: Ernst, R.E. & Buchan, K.L. (eds) *Mantle Plumes: Their Identification Through Time*. Geological Society of America, Special Papers, 352, 291–321.
- Sengor, A.M.C. & Natal’in, B.A., 1996: Paleotectonics of Asia: fragments of a synthesis. In: Yin, A., Harrison, T.M. (Eds.), *The Tectonic Evolution of Asia*. Cambridge University Press, New York, pp. 486–641.
- Surkov, V.S., Trofimchuk, A.A., Zhero, O.G., Kontorovich, A.E. & Smirnov, L.V. 1982: The Triassic rift system of the West Siberian plate and its influence on the hydrocarbon potential of the Mesozoic-Cenozoic platform cover. *Geol. Geofiz.*, 8, 3-15.
- Surkov, V.S., Devyatov, V.P., Zhero, O.G., Kazakov, A.M., Kramnik, V.N. & Smirnov, L.V. 1993: The Earth’s crust structure in the region of the Tyumen’ superdeep borehole. *Geol. Geofiz.*, 1, 120-126.
- Surkov, V.S. & Zhero, O.G. 1981: Basement and development of the platform cover of the West Siberian platform. *Nedra, Moscow* p. 142 [in Russian].

- Surkov, V.S. 2002: Neogean evolution of the young Ural–Siberian platform. *Geologiya i Geofizika*, 43, 754–761.
- Tapley, B., Ries, J., Bettadpur, S., Chambers, D., Cheng, M., Condi, F., Gunter, B., Kang, Z., Nagel, P., Pastor, R., Pekker, T., Poole, S. & Wang, F. 2005: GGM02 - An improved Earth gravity field model from GRACE. *Journal of Geodesy*. DOI 10.1007/s00190-005-0480-z.
- Tscherning, C.C., Forsberg, R. & Knudsen, P. 1992: The GRAVSOFIT package for geoid determination. Proc. 1. Continental Workshop on the Geoid in Europe, Prague, May 1992, pp. 327-334, Prague.
- Verhoef, J., Roest, W.R., Macnab, R. & Arkani-Hamed, J. 1996: Magnetic Anomaly Data of the Former USSR. Geological Survey of Canada Open File Report, 3125a.
- Vyssotski A.V., Vyssotski, V.N. & Nezhdanov, A.A. 2006: Evolution of the West Siberian Basin. *Marine and Petroleum Geol.*, 23, 93-126.
- Wessel, P., & W. H. F. Smith, 1998: New, improved version of Generic Mapping Tools released. *EOS Trans., AGU*, 79 (47), p. 579.
- Wienecke S., Braitenberg C. & Götze H.-J. 2007: A new analytical solution estimating the flexural rigidity in the Central Andes. *Geophys. J. Int.*, 169, 789-794, doi:10.1111/j.1365-246X.2007.3396.x.
- Yardley B.W.D. 1989: An introduction to metamorphic petrology. Longman Scientific & Technical, Essex U.K.

## FIGURES

- Figure 1.1** *Pressure-temperature diagram for some important metamorphic facies (after Yardley, 1989). Also shown is the temperature distribution of the North German basin (Brink, 2005).*
- Figure 2.1** *West Siberian Basin: basin geometry (Vyssotski et al. 2006). The basin is outlined with the bold black line; the northward extent of the basin is not defined according to Vyssotski et al. (2006).*
- Figure 3.1** *Topography of the West Siberian Basin area. Coastline and rivers (purple), basin outline (bold black). Also shown are regional seismic profiles (thin black) used later and the proposed graben-rift structures (grey; after Pavlov, 1995). Names of graben-rifts: K-U, Koltogory-Urengoi; Khs, Khudosei; Kht, Khudottei; A, Agan; U'T, Ust' Tym; Ch, Chuzik.*
- Figure 3.2** *Amplitude of gravity errors of the GGM02C and the EGM96; computed from the standard deviation coefficients of the models.*
- Figure 3.3** *Resolution power of the GRACE gravity field in the estimate of Moho undulations. Set of curves pertain to average Moho-depths between 30 and 70 km. The curves were obtained by inverting the accumulated error curve for GRACE and EGM96 (Figure 3.2). Density contrast at the Moho boundary: 500 kg/m<sup>3</sup>. The resolution is even better for smaller densities.*
- Figure 3.4** *Moho depth map for the West Siberian Basin area, digitised from Vyssotski et al. (2006) based on an older work by Kovylin (1985). Basin outline (bold black) and 200 m topography isoline (thin black). Black lines show regional seismic profiles. Coastline and rivers (blue).*
- Figure 3.5** *Sediment thickness map from Statoil database. Basin outline (bold black) traced along the 500 m isopach line. Thin black lines show regional seismic profiles.*
- Figure 3.6 a** *Southern West Siberian Basin sector: Total sediment thickness (red) from Statoil database and horizon separating the pre-volcanic and the post-volcanic sedimentary rocks (blue), digitized from Vyssotski et al. (2006).*
- Figure 3.6b** *Northern West Siberian Basin sector: Total sediment thickness (red) from Statoil database and horizon separating the pre-volcanic and the post-volcanic sedimentary rocks (blue), digitized from Vyssotski et al. 2006.*
- Figure 4.1** *Experimental depth dependency of the TWT for regional seismic profiles 06 (red dots) and 19 (discs with crosses). The interpolated curve is used to convert the horizons given in units of TWT to depths.*
- Figure 4.2** *a) Velocity of sediments in function of depth. The relation was found from the analysis of the TWT. b) Comparison of the a-priori depth-dependent linear density increase with the density corresponding to the above velocities. Different relations were used for calculating the relation of density to velocity (Nafe-Drake (Ludwig et al., 1970; Jones, 1999), Gardner's rule (Gardner et al. 1974), and Hamilton's relations (Larsen et al. 1994).*

- Figure 5.1** Free-air gravity anomaly ( $mGal = 10^{-5} m/s^2$ ) for the West Siberian Basin area. (Data: EIGEN-GL04C, Förste et al. 2006). Coastline and major rivers in blue. Isoline interval 15 mgal. Basin outline (bold black). Topography 200 m isoline (thin black). Also shown are regional seismic profiles and the proposed graben-rift structures (grey; after Pavlov, 1995). Names of graben-rifts: K-U, Koltogory-Urengoi; Khs, Khudosei; Kht, Khudottei; A, Agan; U'T, Ust' Tym; Ch, Chuzik.
- Figure 5.2** Bouguer gravity anomaly ( $mGal$ ) for the West Siberian Basin area. (Data: EIGEN-GL04C, Förste et al. 2006). The linear gravity highs are marked by black arrows.
- Figure 5.3** Geoid residual (m) for the West Siberian Basin area. Data: EIGEN-GL04C (Förste et al. 2006) freed from lowest degree and order (up to degree and order 10) harmonic components.
- Figure 5.4** Geoid residual terrain corrected (m) for the West Siberian Basin area. Data: EIGEN-GL04C (Förste et al. 2006) freed from lowest degree and order (up to degree and order 10) harmonic components. A: geoid low correlates with the deepest part of the basin. B, C: geoid highs correlate with shallow basement.
- Figure 5.5** Gravity effect of sediment-package. Linear density increase with depth.
- Figure 5.6** Gravity residual: Bouguer anomaly reduced for the sediment package. Linear density increase with depth of sediments. Seismic lines and supposed graben-rift structures as in Fig. 5.1.
- Figure 5.7** Gravity effect caused by density contrast at the Moho interface. Reference depth =35 km, density contrast:  $0.35 kg/m^3$ . Seismic lines and supposed graben-rift structures as in Fig. 5.1.
- Figure 5.8** Gravity residual: corrected for topography, sedimentary rocks and crustal thickness variations. Moho reference depth=35 km, Moho density:  $350 kg/m^3$ . Also shown are regional seismic profiles and the proposed graben-rift structures (grey; after Pavlov, 1995). Names of rifts: K-U, Koltogory-Urengoi; Khs, Khudosei; Kht, Khudottei; A, Agan; U'T, Ust' Tym; Ch, Chuzik.
- Figure 5.9** High pass filtered gravity residual, including the correction of the Bouguer anomaly for sedimentary rocks and crustal thickness variations. Also shown are regional seismic profiles and the proposed graben/rift structures (grey; after Pavlov, 1995). Names of rifts: K-U, Koltogory-Urengoi; Khs, Khudosei; Kht, Khudottei; A, Agan; U'T, Ust' Tym; Ch, Chuzik.
- Figure 5.10** Low pass filtered gravity residual, including the correction of the Bouguer anomaly for sedimentary rocks and crustal thickness variations. Seismic lines and supposed rift structures as in Fig. 5.1.
- Figure 5.11** Tentative map of the depth to the base of the basalt layer – the depth is only constrained along the profiles shown in the figure. Seismic lines and supposed graben-rift structures as in Fig. 5.1.

- Figure 5.12** *Tentative estimate of the order of magnitude of the gravity signal produced by the basalt layer. Seismic lines and supposed graben-rift structures as in Fig. 5.1.*
- Figure 6.1** *Lower crustal density variations calculated by inverting the residual gravity signal (Fig. 5.8). The density variations are assumed to be in a lower crustal layer extending from the Moho to 20 km upwards. Seismic profiles and supposed -rift structures as in Fig. 5.1.*
- Figure. 6.2** *Upper crustal possible basalt layer obtained by inverting the high-pass filtered residual gravity signal (Fig. 5.9). The masses are assumed to have a density contrast of  $300 \text{ kg/m}^3$  to the surrounding basement and being located at a reference depth of 5 km. Negative thicknesses are equivalent to a layer of equal thickness but with a negative density contrast.*
- Figure 6.3** *The gravity field produced by the crustal model including sedimentary rocks, crustal thickness variations, upper crustal masses (wavelengths between 50 and 150 km), and lower crustal density variations (wavelengths greater than 150 km). Compare to the Bouguer anomaly (Fig. 5.2).*
- Figure 7.1** *Isostatic Moho, considering the sedimentary and the topographic load. Reference depth = 35 km.*
- Figure 7.2.** *Isostatic gravity anomaly.*
- Figure 8.1** *Bottom of pre-volcanic sediments with interpretation of segments composing the basin and principal rift-graben structures.*
- Figure 8.2** *Magnetic anomaly of the West Siberian Basin (data from National Geophysical Data Center, 1997).*